UNIVERSIDADE DE SÃO PAULO

ESCOLA DE ENGENHARIA DE SÃO CARLOS

YORMARY NATHALY COLMENARES CALDERON

The effect of morphology and cobalt concentration on the sensing properties of zinc oxide sputtered films

São Carlos

2018

YORMARY NATHALY COLMENARES CALDERON

The effect of morphology and cobalt concentration on the sensing properties of zinc oxide sputtered films

(Versão Final Corrigida)

Dissertação apresentada ao programa de Pós-Graduação em Ciência e Engenharia de Materiais da Universidade de São Paulo, para obtenção do título de Mestre em Ciências.

Orientador: Valmor Roberto Mastelaro

Área de concentração: Desenvolvimento, Caracterização e Aplicação de Materiais.

São Carlos

2018

FOLHA DE JULGAMENTO

Candidata: Licenciada **YORMARY NATHALY COLMENARES CALDERON.**

Título da dissertação: "Efeito da morfologia e concentração de colbato nas propriedades sensoras dos filmes de óxido de zinco depositados por *sputtering*".

Data da defesa: 22/03/2018.

Comissão Julgadora: **Resultado:**

Prof. Associado **Valmor Roberto Mastelaro**   *Aprovado*
(Orientador)
(Instituto de Física de São Carlos/IFSC)

Prof. Dr. **Marcelo Orgaghi Orlandi**   *Aprovado*
(Escola Estadual Paulista "Júlio de Mesquita Filho"/UNESP- Araraquara)

Prof. Associado **Fernando Josepetti Fonseca**   *APROVADO*
(Escola Politécnica/EP-USP)

Coordenador do Programa de Pós-Graduação em Ciências e Engenharia de Materiais:
Prof. Associado **Antonio José Felix de Carvalho**

Presidente da Comissão de Pós-Graduação:
Prof. Associado **Luis Fernando Costa Alberto**

Al señor papá y a la señora mamá

Agradecimentos

Em primeiro lugar, gostaria de agradecer profundamente ao prof. Dr. Valmor Mastelaro por me aceitar como sua estudante de mestrado, proporcionar a infraestrutura e criar oportunidades para meu crescimento como pesquisadora. Obrigado professor por todo carinho e paciência durante meu trabalho.

Meus sinceros agradecimentos ao Brasil e a CAPES pela oportunidade de desenvolver meu mestrado aqui. Não são todos os países que recebem tão abertamente estrangeiros e oferecem tal oportunidade de bolsa.

Aos técnicos e colegas do Grupo de Crescimento de Cristais e Materiais Cerâmicos do Instituto de Física de São Carlos pelo apoio técnico. Agradeço em especial a Dalila e Lucas Francisco pelos bons momentos e conversas de laboratório.

Gostaria de exprimir minha gratidão ao prof. Dr. Adenilson Chiquito, o qual ajudou me imensamente com as medidas de resistividade elétrica e contribuiu com discussões importantes sobre o modelo de condutividade em materiais porosos. Obrigada por me escutar e discutir minhas idéias.

A Wagner Correr, por todas as horas de discussão científica produtivas, suas ideias contribuíram substancialmente para este trabalho. Agradeço pela ajuda na parte experimental e pela paciência em escutar minhas ideias. Acima de tudo, por me fazer acreditar em minha capacidade como pesquisadora.

Aos meus pais, Rigoberto e Nancy, e as minhas irmãs, a Gordita e a Unicórnio, por todo amor e carinho que vocês me mandaram desde tão longe. Sem o apoio de vocês a vida teria sido mais difícil por aqui.

Finalmente, e não menos importante, aos grandes amigos Rafael Paiotti e Bruno Castilho pelos agradáveis momentos dentro e fora da Universidade. Rir com vocês fez meu mestrado muito mais divertido aqui em São Carlos.

Solo una cosa convierte em
impossible un sueño:
el miedo al fracasso.
Los cuentos de Nasrudin

RESUMO

COLMENARES CALDERON, Y. N **Effeito da morfología e concentração de cobalto nas propriedades sensoras de filmes finos de oxido de zinco por sputtering.** 78p. Dissertação (Mestrado) –Escola de Engenharia de São Carlos, Universidade de São Paulo, São Carlos, 2018.

O uso de materiais semicondutores aplicados como dispositivos sensores é atualmente um dos tópicos mais pesquisados na área de controle da qualidade do ar e proteção ambiental. As pesquisas são focadas na produção de novos materiais sensores com limites de detecção, seletividade, temperaturas de trabalho e tempos de resposta, melhores que as apresentadas pelos materiais já conhecidos. Embora os modelos teóricos mostrem a grande importância da morfologia na detecção de gases, uma relação direta entre a estrutura, tamanho/morfologia e as propriedades sensoras não tem sido experimentalmente estabelecidas na literatura. Neste trabalho, *sputtering* de rádio frequência é utilizado para depositar e produzir filmes finos de oxido de zinco a partir de alvos cerâmicos e metálicos, em que o último é submetido à oxidação térmica para obter filmes porosos de ZnO. As amostras são depositadas em interdigitados de platina e foi estudado o seu comportamento elétrico quando é exposto a ozônio. Os efeitos de tamanhos de estrutura e porosidade dos filmes são estudados em relação à melhoria da resposta sensora. Os resultados obtido mostram que os sensores com tamanhos de estrutura menores e baixa porosidade apresentam baixa sensibilidade e rápidas respostas; no entanto, as estruturas maiores em filmes altamente porosos exibem baixas sensibilidades e maiores tempos de resposta. O melhor desempenho sensor encontra-se em um ponto médio em que a aparente área superficial para adsorção é maximizada e é registrada a melhor reposta ao ozônio. Por outro lado, o comportamento elétrico dos filmes dopados demonstrou que a presença de cobalto desempenha um papel fundamental. Com a inserção de cobalto, a resposta sensora foi melhorada em 62% sob as mesmas condições de medida. Porém, o aumento das concentrações de cobalto modificaram a condutividade do oxido de zinco para comportamentos tipo-p e diminuiu drasticamente a resposta do sensor, devido a possível segregação de óxido de cobalto. Os nossos resultados propõem o método de deposição RF-Sputtering como uma técnica versátil na produção de sensores semicondutores para gases, uma vez que a porosidade e assim a sensibilidade pode ser controlada por meio da deposição de metais e dopantes seguido por oxidação térmica.

Palavras-chave: Sensor de gás, Sputtering, Óxido de zinco, Ozônio, Filme fino.

ABSTRACT

COLMENARES CALDERON, Y. N **The effect of morphology and cobalt concentration on the sensing properties of zinc oxide sputtered films.** 93p. Dissertação (Mestrado) –Escola de Engenharia de São Carlos, Universidade de São Paulo, São Carlos, 2018.

The use of semiconductor materials applied in gas sensing devices is currently one of the most researched topics in air quality control and environmental protection. The research is focused on the production of new sensing materials with improved detection limits, selectivity, working temperatures and response times of the known semiconductor materials. Although theoretical models show the great importance of morphology on gas detection, a direct relation between structure size/morphology and the gas sensing properties has not been experimentally established. In this work, Radio Frequency-sputtering method is used to deposit and produce zinc oxide thin films from ceramic and metallic targets, in which the latter are submitted to thermal oxidation to obtaining ZnO porous films. The samples are deposited on platinum interdigitated electrodes and the electrical behavior is analyzed when exposed to ozone. The effects of feature size and film porosity are studied regarding the enhancement of sensor performance. The results show sensors with small features and low porosity present low ozone sensitivity and fast response; while greater features in highly porous films exhibit low sensitivity and slower responses. The optimum sensing performance is found to be somewhere between when the apparent surface area available for adsorption is maximized and the best ozone response is registered. On the other hand, the electrical behavior of doped films when exposed to ozone demonstrates cobalt presence plays a fundamental role. By inserting cobalt, we could improve the sensor response by 62% under the same conditions. However, the increase of doping concentration modify the zinc oxide conductivity to p-type and drastically decrease the sensor response due to the possible formation of cobalt oxide segregates. Our results propose RF sputtering deposition as a versatile technique in the production of semiconductor gas sensors, once high porosity and, therefore, sensitivity can be controlled through the deposition of metals, and dopants, followed by thermal oxidation.

Keywords**:** Gas sensor, Sputtering, Zinc oxide, Ozone, Thin film.

Table of Contents

1 INTRODUCTION

In the last decades, the development of gas sensing devices has become an important issue in the research field of semiconductor materials and thin films. The number of scientific papers concerning semiconductor with gas sensing properties has been increasing by almost 20% per year (since 2011) due to the expanding demand for selective gas sensors with very low detection limits [1–4].

The numerous sensor applications range from security equipment in the industry to disease diagnostic [5–7] and are mostly related to the risk that some gases as NO, CO, NO_2, NH, and O_3 can represent to human health [8–10]. The *Air quality and health* reports of the World Health Organization explain how prolonged exposure to toxic gases may cause irreversible deterioration of cardiovascular, respiratory and/or nervous system, specifying the harmful pollution levels of gases concentrations, at levels that go from parts per million to parts per billion [11]. Currently, the detection of specific gases resulting from industrial or biological processes, (as the high acetone levels exhaled by patients suffering for diabetes [6]) is of extreme interest as a tool for air quality, control safety and medical diagnostic.

Although there is a wide variety of commercial sensor devices, each one depending on different operation mechanism (absorption of infrared radiation, oxidation/reduction of an electrode, i.a.), there are problems related to gas specificity, detection limits and production costs which could be solved using semiconductor surfaces. The most used semiconductor materials in gas sensing, e.g, tin oxide (SnO_2), tungsten dioxide (WO_3), zinc oxide (ZnO) and indium oxide (In_2O_3), have the capacity to measure low concentration of pollutant gases (ppm to ppb) maintaining low production costs at relatively elementary systems composed by an electrode system and a thin film of semiconductor material [3]. The sensing properties of these materials reside on the surface interactions that take place at the gas-solid interface [12]. When a gaseous species is in contact with a semiconductor's surface, it could be trapped/adsorbed by the formation of a chemical bonding. The interaction leads to a change in the number of semiconductor's charge carriers, which modifies the materials electrical conductivity. Therefore, in such systems the gas detection only requires a 2D distribution of the semiconductor material (thin film form) disposed between electrodes for the recording of resistance changes.

Although semiconductors are materials with recognized gas sensing capacity and

appealing simplicity, there are still problems related to the lack of gas selectivity, the magnitude of the response to low gases concentration (operation range), the response speed and the high operating temperatures, which maintain the research in the field very active in search of new materials with enhanced sensing properties. Currently, the frontier in this research area has been established at the enormous not understood influence that morphology, crystallinity, type of semiconductor material and dopant presence, have in semiconductor sensor properties [4,13].

As composition and structure variations modify the electronic band structure of materials, dopant presence also alter the electrical behavior of films and conduction mechanism. Problems with the lack of selectivity have been solved for instance, when doping semiconductor materials as zinc oxide (ZnO) and tungsten dioxide (WO_3) with some transition metals [14–17]. Likewise, studies have demonstrated that hierarchical structures and some nanostructures improve the sensibility of widely used materials such as SnO_2 and WO_3, enhancing the performance of sensors at room temperature significantly [18–21].

Even though there is an extensive number of projects and efforts focused on developing efficient gas sensors, the problems and limitation in semiconductor gas sensing persist. The principal obstacle is our limited understanding of the practical mechanisms responsible for sensing, the electric conduction in thin films and the dopant role in gas detection [22].

According to *Barsan and Weimar* [12], there is a huge gap between the approach of gas sensing developers, who empirically optimize the sensor properties, and basic research scientists whose purpose is to describe the gas sensing mechanisms. Despite theoretical models show the dependence of semiconductor sensing response with aspects as superficial area, grain interconnection and thickness of depletion layer, almost none of the experimental studies attempt to understand the physics behind the detection process and establish direct relations between those factors and gas sensing. The main reasons for this are the experimental limits and complexity of finely controlling the thin film growth and composition, regarding doping levels and film morphology.

Considering the challenges in developing a new sensing material while studying the physical phenomenon, the objective of this work is to propose the use of a synthesis/deposition technique that allows controlling morphology and composition in a very accurate way. The method to be used, the sputtering technique, is a physical deposition method known primarily for the formation of uniform films and that has not been very explored in the gas sensing development. The stability of the process, the relatively low cost and the possibility of control

almost every parameter during film deposition, make this technique a potential tool for sensing design of nanostructured films [23].

On the other hand, since the sensing mechanism involves adsorption of gaseous species, it is expected that variations of the number of adsorption sites would change the sensor electrical response. One way to induce this effect is change the micro/nano-structure, which can bring modifications at the surface energetics and the adsorption sites number. Our objective is to use the film growth conditions of the sputtering method, to study different morphologies and compositions in terms of adsorption sites available for gas detection at zinc oxide (ZnO) semiconductor surface. Currently, the ZnO easy/low-cost synthesis, and the magnitude of the pure material response (comparable with the performance of materials commercially available), make him a potential tool for gas sensing progress and one of the most researched materials [24].

In this study, we present the gas sensing characteristics of pure and cobalt doped ZnO films, as well as how distinct morphologies can affect the gas sensing response. After a brief revision presented in chapter 2 about significant papers on which this work was based, the methodology of the work is described.

2 LITERATURE REVIEW

2.1 Semiconductor gas sensors: How it works?

A semiconductor electrical behavior is determined by band gap energy and by the density and type of charge carriers. At n-type semiconductors, the number of negative charge carriers is greater than positive ones, making the electrons the responsible for the electrical conductivity. Otherwise, conductivity in p-type semiconductors is through electron holes (positive charge carriers), the major carrier.

In any semiconductor with gas sensing properties (n or p type), the number of charge carriers varies as result of the interaction of the material surface with the gaseous phase. When an atom/molecule is physically adsorbed on the material surface, a chemical bond is formed; to do this, the surface shares electric charge with the adsorbate (atom or molecule) leading to a change in the number of semiconductor charge carriers. The adsorptive species capture electrons or electron holes from the conduction band, acting as a source or sink of charge carriers depending on the conduction mechanisms [25].

When the surface interaction is with oxygen atoms specifically, it appears a space-charge layer as a result of adsorption of the oxygen atoms wich capture electrons from the conduction band (ion formation O^-), leaving a positive electron hole and a surface electron-depleted region [2], as schematized bellow.

$$O_{gas} + e^-_{cond.\ band} \rightarrow O^-_{adsorbed} \qquad (1)$$
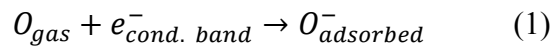
For n-type semiconductors, the trap of electrons by the adsorbate atoms leads to a decrease of charge carriers available for electrical conduction. On the contrary, oxygen adsorption on p-type semiconductor leads to an increase in conductivity, due to the positive electron holes created at the semiconductor surface. For reductive species, the effect is on the other way: the gaseous atoms interact with the surface oxygen releasing it and allowing the transfer of the negative charge to the semiconductor. This increase the number of electrons in the conduction band and reduce the number of electron holes. In this sense, the variation in electrical conductivity is directly related with the type of the species in the gaseous state and the nature of the semiconductor surface [17,26,27].

Moreover, gaseous species must overcome an energy barrier to be adsorbed. Such

barrier is known as Activation Energy for Adsorption and it is related to the existence of optimum operating temperature. The reason is that at low temperatures, the barrier energy for adsorption is high and the probability of capture gaseous species in the surface is low. As the temperature rises the potential barrier decreases; however, the probability of surface desorption is higher, decreasing the surface residence time and this the surface-gas interaction. Therefore, the optimum operating temperature is a compromise between the adsorption and desorption processes, which are limited by the activation energy and residence time, respectively.

Conduction in thin films

In the gas sensing mechanism stated before, the sensitive layer is the electron depleted (or hole depleted) region near the surface of the semiconductor grains [12] (darker blue in Figure 1). This sensitive layer and the inter-grain connection are responsible for transducing the gas adsorption into a measurable electrical signal. The connectivity between grains, their shape and morphology will affect not only the total amount of sensitive layer present in a material, but also the gas sensing property, which is, strongly dependent on the film morphology. According to the conduction and response models for metal oxide gas sensors [3,12,22,28] the conductivity of a grain network is controlled by the resistance of inter-grain contacts, while the capacity of interaction with the gaseous species is determined by the surface energetics and the area accessible for adsorption.

Depending on the morphology of the thin film structure, sensing will occur in different numbers of adsorption sites. A compact film, for example, would have a smaller number of adsorption sites than a porous film, consequence of the smaller surface area active for adsorption (see Figure 1). A different feature affecting gas sensing is the bulk surface ratio; films with bulk-surface ratio large enough for surface reactions do not affect the conductivity of bulk, will present a limited sensibility.
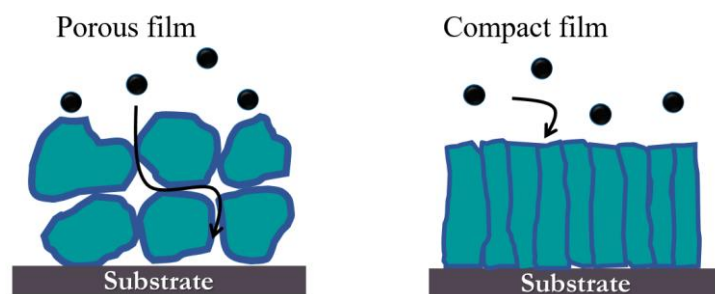
Figure 1 Scheme of the gas interaction according surface area in porous and compact films. Source: by the author.

Barsan and Weimar developed a conduction model for porous films considering the grain charge layer created by gas adsorption [12]. They represent the electrical resistance of a porous film as a circuit with a large number of resistances (grains/structures) connected in series.

From the semiconductor band theory perspective, the lack of electrons (after adsorption) at the conduction band produce a band bending which length is the depletion layer thickness λ_D (Figure 2b). As all grains at the active surface would have a depletion layer, the conductivity of a grain network would be restricted by the presence of a surface barrier at the interconnection between grains as shown in Figure 2c. The height of this potential barrier depends on the depletion layer thickness and grains connectivity. Accordingly, it is possible to consider three general cases for inter-grain conduction:

- Large grains with completely depleted contacts: *Large grains* refers to grains which size is larger than the depletion layer thickness. The case of completed depleted contacts appears when the grains are not sintered together; in such situation there is not an overlapping of the structures and the neck region is active for adsorption (Figure 2d). This creates the potential barrier known as the Schotky barrier.

- Large grains with partly depleted contacts: In this case, the contact is not gas sensitive due to the neck formation (Figure 2e). The inter-grain conduction depends on the relative dimensions of depletion layer and neck [12]. For narrow necks, the influence of depletion layer would introduce an additional potential barrier in charge transport; further, necks large enough will allow inter-grain conduction in the same way a bulk material does.

- Small grains: The small grains include those grains which dimensions are smaller or comparable with the depletion layer. Here the gas adsorption change the material conductivity without dealing with surface-bulk effects since the material electrical resistance is entirely the resistance at the surface. At this scale, the mean free path of charge carriers becomes important and the number of surface collisions principally affects the material resistance.

At the same time, the conduction mechanism will vary from one case to another as the depletion layer thickness changes. In the presence of an oxidative atmosphere, the depletion region will become thicker until the occupation of all adsorption centers, while reductive gases will make such layer thinner. A detailed description of the depletion layer behavior in presence of different gases reactions is presented by Barsan [12].
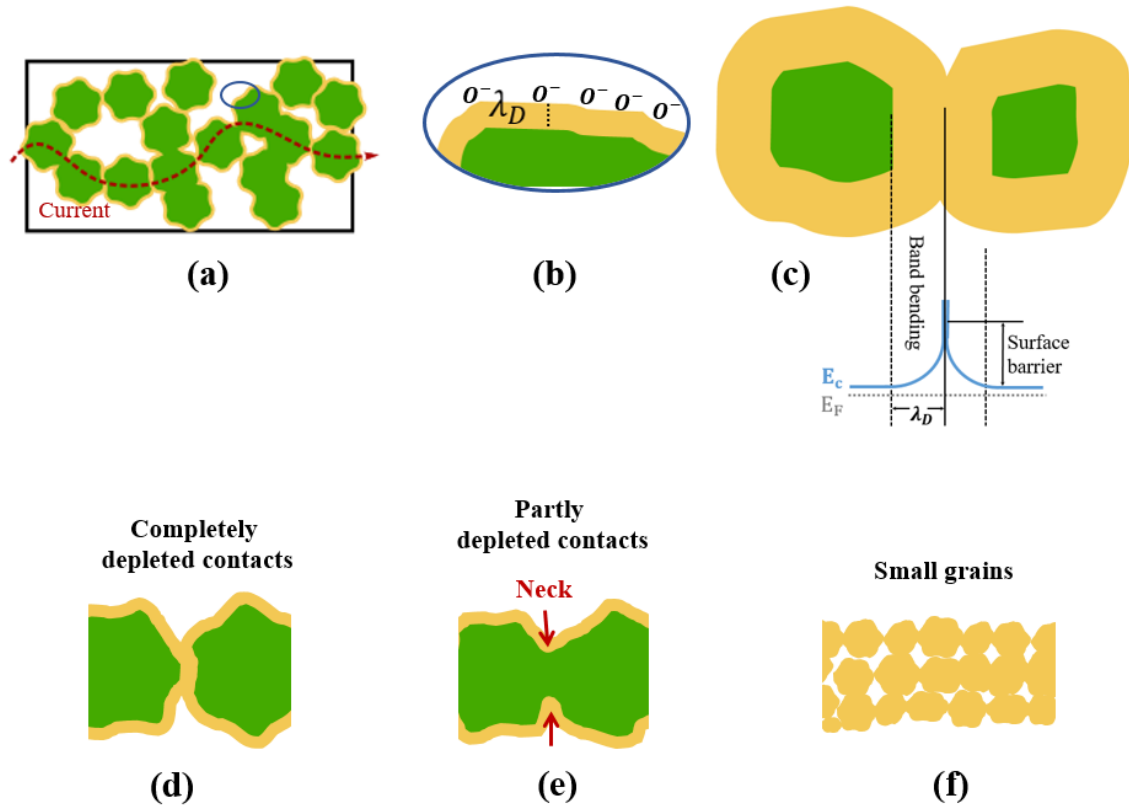
Figure 2 Models for electrical conductivity between grains in porous films. The current flow between grains of porous films (a) is affected by the formation of a potential barrier in grains interconnection (c) formed by the depletion layer after oxygen adsorption on grain surface (b). The electron flow experiments different barrier according to the grain connections: completely depleted contacts (d), partly depleted contacts (e) and small grains where the grain size is near the depletion layer thickness. Source: by the author.

To conclude, films from the same semiconductor material may present different responses to gas presence according to the size of the structures and the overlapping of grains. The combined effects of large areas suitable for adsorption and the contact between grains are fundamental to improve the gas sensor properties of semiconductor materials.

2.2 Zinc oxide compound

In 1962, zin oxide thin films were the first materials reported to change conductivity due to interactions with gaseous phase [29]. This direct band gap semiconductor has been used in a wide range of applications due to his optical, electrical and catalyst properties. As others wide band gap materials (3.37eV) the high electron mobility, field strength and exciton binding energy make it a promising material for development of transparent electronic and spintronic

devices, UV/Vis emitters, and sensor materials [30].

The most common and stable crystal structure of zinc oxide is the compact hexagonal structure known as Wurtzite, where zinc ions (Zn^{2+}) are tetrahedrally coordinated with 4 oxygen atoms, which density is *5.605g/cm³*[31]. Zinc oxide is typically found as n-type semiconductor due to the intrinsic native donor defects: interstitial zinc and oxygen vacancies, where these last are the most abundant because the favorable energy formation [32]. Therefore, the oxygen vacancies and interstitial zinc drive the electrical and catalytic properties of ZnO, acting as electron donor or adsorption center respectively [31]. By increasing of the charge carriers number, it is possible to improve the electrical conductivity of n-type zinc oxide. Some studies have performed the doping of ZnO with metals such as aluminum, gallium and indium, achieving a significant increment in the charge carrier concentration and producing one of the transparent materials with highest conductivity available today [30,33–36].

Although less common, p-type zinc oxide also represents great technological interest due to the promissory use for a p-n junction UV LED. As native defects can form spontaneously and cancel the dopant acceptors impurities, synthesis of p-type ZnO semiconductor is experimentally difficult. Nevertheless, abundant experimental results show that doping ZnO with elements from groups V, IV and I lead to the formation p-type material with good stability and enhanced performance.

One of the advantages of working with zinc oxide is the variety of routes to obtain it in Wurtzite phase. The synthesis methods and growth mechanisms go from vapor liquid-solid mechanisms (VLS) to aqueous solution growth (ASG), where the sol gel-process, the polymeric precursor and, hydrothermal, are the three most common methods. According to the precursors used, treatment conditions and processing, ZnO assume a great variety of morphologies, as nanobelts, nanotrees, nanoneedles, microplates and the most usual, the ZnO nanorods [37]. The disadvantage when working with this metal oxide, resides in the complexity of finely controlling the characteristic dimensions in ZnO microstructures, allied with its great reactivity with the air humidity [31].

2.3 ZnO compound as gas sensor

Although the adsorption of gaseous species in metal oxide is still not entirely understood, some authors affirm that the predominant mechanism responsible for gas adsorption is vacancies of oxygen in the material surface [26]. Whether this is completely true or

only partially, the native oxygen vacancies and the high catalytic activity of ZnO, place it as one of the most interesting materials for the development of new gas sensing devices.

Experimental studies have shown that the gas sensing response of ZnO is comparable with the performance of the most used materials for this purpose, becoming even superior when doped or in nanocomposites [24]. As other sensing materials, the ZnO composition (dopants, defects, etc) and thin film nanostructure have a fundamental role in the determination of the response magnitude, the range of operation, working temperature and selectivity [38,39].

As explained previously, there is a great variety of morphologies that ZnO can assume, each one has shown distinct sensing properties according to the surface reactivity and electrical properties [24]. In the work of Alenezi et all [19], ZnO hierarchical structures exhibit improved gas sensing performance compared with mono-morphological ZnO and commercial ZnO powders. Similar to the behavior of other sensing materials [18], the greater sensitivity and reduced response speed of this structures are attributed to the high surface-volume ratio and formation of secondary junctions of this nanostructured films.

In the *modified grain model* of Barsan et al [12], the importance of grain structure is another critical parameter with great impact on the sensing mechanism. Their model predict an increment in the sensor response as grain sizes approach to the width of the depletion layer. Differently, the work of Korotcenkov et al [22] shows that it is experimentally impossible to settle this as a conclusion for all materials. Depending on the type of semiconductor and detected gas, the grain size would have a greater or lesser (even zero) influence on sensor response. Korotcenkov affirms that sensing mechanism is the product of several features and the grain size influence is not explicit for all materials. Particularly for ZnO, the influence of grain size is depicted by the experimental study of Xu et al [40]. They calculated the crystallite size of a synthesized powder by the *Debye-Scherrer* method and found that, for different gases, decreasing in the grain size brings a substantial increment in material's sensibility.

Along with morphology and grain size, the zinc oxide composition serves as another route to change the gas sensing properties. Recently, experimental studies have shown doping ZnO with metals as niobium and aluminum enhance sensing and electrical properties, presenting higher responses and lower working temperatures [38,41].

Furthermore, doping with some others transition elements has demonstrated to cause an effect of selectivity in ZnO thin films. This was investigated by Darvishnejad et all [15], who synthetized ZnO plates by the hydrothermal method and doped them with manganese, iron,

cobalt and nickel. In their work, cobalt doped films present an improved selectivity to ethanol, while nickel and manganese doped films show certain selectivity to acetone.

Particularly, Co doping seems to have a major effect on the gas selectivity of materials as tungsten trioxide and aluminum/indium lanthanum silicate [16,42]. For zinc oxide, the effect of cobalt doping is still matter of study; in contrast with the results of Darvishnejad et all[15], other studies indicate doping ZnO with cobalt would have different effects according to the cobalt concentration and synthesis method [14,43].

A detailed study of cobalt doping and its influence on ZnO gas sensing characteristics is presented by Catto et al [43]. According to the results obtained for Co-doped ZnO by polymeric precursor method, the improved sensing performance of ZnO is proportional to the cobalt content (substitution of Zn for Co up to 5% mol). They found, that the cobalt ions Co^{+2} are preferentially replacing the Zn^{+2} sites, which produce a change in the number of oxygen vacancies and change the catalytic activity of ZnO surface, explaining not only the higher responses, but the lower operating temperatures and high selectivity to ozone of the samples

2.4 Sputtering deposition method

One of the major problems in semiconductor gas sensors is the influence that synthesis method has on sensor development. It has been reported that the same metal oxide semiconductor, with similar morphologies, present different sensing properties according to the synthesis and deposition methods used for thin film formation [37]. Indeed, most of the ZnO chemical synthesis methods are extremely sensitive and small variations in synthesis parameters can result in films with slight differences in structure and surface composition [37]; this lack of growth control make almost impossible the reproduction of same sensing results from one film to the other.

Sputtering, in this context, is an appealing technique to obtain such films once it allows high controllability of the process, time saving, low deposition complexity, and film growth stability. Furthermore, due to the higher deposition rates and relatively low temperatures achieved with this technique, the sputtered films have greater porosities (unmatched by almost any other technique) which from the perspective of gas sensor applications represents an extra advantage. Porous films have high surface area available for adsorption that could lead to increments in the sensor response.

The sputtering process consists in the removal of cathode's material (target) by the

bombardment of energetic ions [44]. When ejected from the target, the atoms accumulate on the substrate surface forming a film. The most usual geometry between the target and the substrate is shown in Figure 3. The deposition is performed in a vacuum chamber with a low pressure of the working inert gas. A strong electric field is generated between cathode (target) and anode causing the ionization of the inert gas and the acceleration of the ions toward the target material (sputtering of the target). Depending on the form that the ionizing potential is applied, the sputtering can be classified as direct current (DC) or Radio frequency sputtering (RF). In RF-sputtering, instead of applying a constant voltage between cathode and anode, an oscillating voltage with a high radio frequency is applied. This feature maintains the discharge even for targets of insulating material.
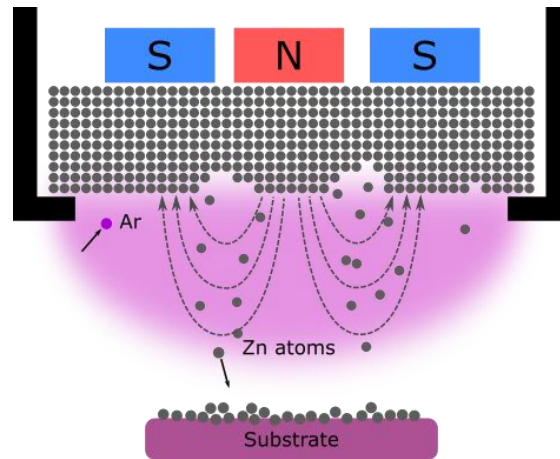
Figure 3 Schematic diagram of the essential parts in a sputtering process. Source: by the author.

Besides the radio frequency, a magnetic field at the target region it is usually used. This is called magnetron sputtering and allows the electrons to travel longer distances, enhancing the ionization process and keeping the plasma concentrated at the target surface.

2.5 Objectives of the present research project

Despite the complexity of experimentally determine the influence of every parameter on the gas sensing phenomenon, the comprehension of such process is essential in order to make advances in this field and to find a solution for the limitations of sensors produced so far. The purpose of this project is to synthesize ZnO thin films by RF Magnetron Sputtering and study the film formation process to optimize sensor properties as a function of microstructure and dopant concentration.

For this purpose, the next specific objectives were established:

- Synthesize ZnO thin films by RF Sputtering from ZnO ceramic target and Zn metallic targets with subsequent thermal oxidation.

- Analyze the influence of film growth conditions in the microstructure and crystallinity of zinc oxide thin films (target material, deposition rate, substrate, dopants presence and thermal treatment).

- Study the microstructure influence in the gas sensor response of undoped ZnO films.

- Synthesize Cobalt doped ZnO films and study the gas sensor response in function of dopant concentration.

3. MATERIALS AND METHODS

The work scheme followed during this research project is shown in Figure 4. All experimental work is divided into three important sections: thin film deposition, structural and chemical characterization and, finally, the validation of gas sensing properties. At the first part of the work, the film growth of sputtered films and its influence in the morphology of ZnO films is studied. To find the deposition conditions that improve the sensing properties, the response to ozone of ZnO sputtered films are investigated. Finally, deposition conditions of the ZnO sensor with good response are reproduced for the synthesis of doped ZnO films and study of cobalt concentration influence.
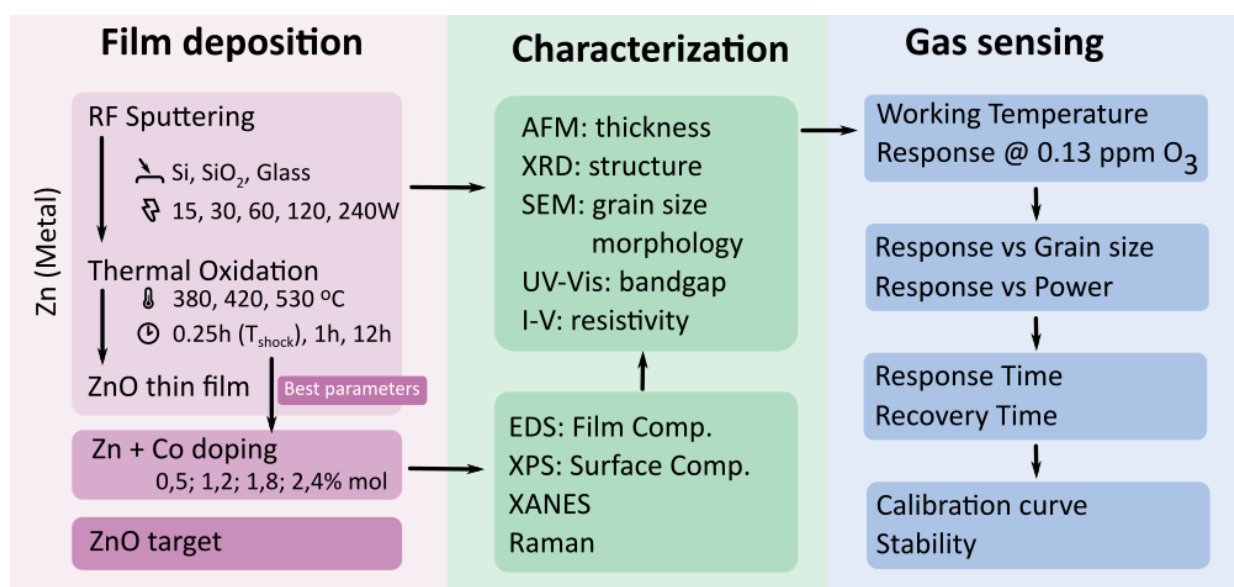
**Figure 4** Work plan scheme for the study of sputtered ZnO films used as a gas sensor. Source: by the author.

3.1 Thin Film Deposition

All the films were obtained by the sputtering of pure zinc metal or the ZnO ceramic target in an RF-magnetron sputtering system operating at a radio frequency of 13.5 MHz and a background pressure of low 10^{-6} mbar. The equipment components distribution is the showed in Figure 3. The vacuum chamber was previously pumped to the base pressure and then, the chamber pressure is raised to the working pressure of 2×10^{-2} mbar by injecting argon. Films were deposited with power ranging from 15 to 240W and over substrates of silicon, silica wafers and glass, all cleaned with RCA cleaning process. The film's thickness was monitored with a

quartz crystal sensor inside of the chamber.

To obtain zinc oxide films from metallic Zn depositions, the metallic films were oxidized in a furnace with air atmosphere. It was studied distinct temperatures and times to achieve complete oxidation (see Figure 4).

For uniform cobalt addition, it is necessary to perform the sputtering of zinc and cobalt simultaneously. To achieve it, cobalt strips were placed on the zinc target area, each strip occupying 2.3% of the total (See Figure 5). By varying the number of cobalt pieces, it is possible to achieve different levels of cobalt doping corresponding to 4, 3, 2 and 1 strips respectively.
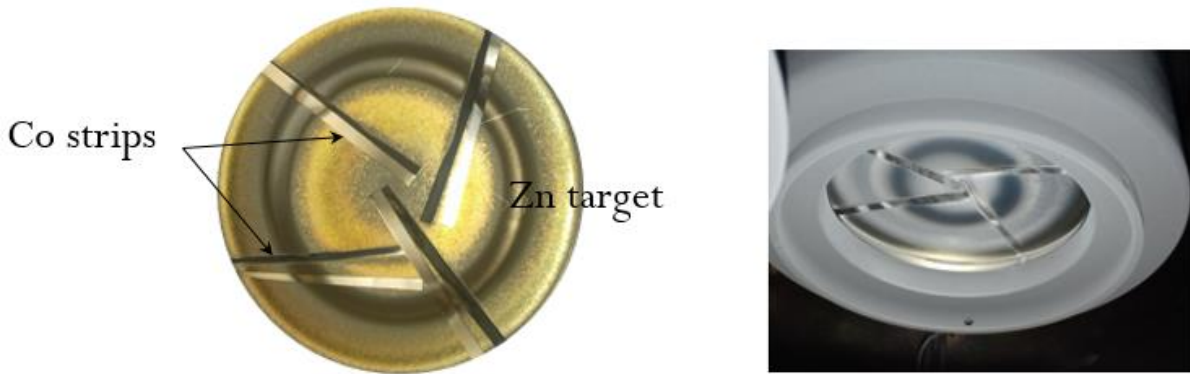
Figure 5 Pictures of the zinc metallic target with the four cobalt strips. Source: by the author.

The nominal doping concentration is calculated as the ratio of cobalt sputtered atoms and total sputtered atoms (Zn+Co atoms). Since the target is symmetrically sputtered, the number of removed atoms for a given element is proportional to the sputter yield (specific for each element) and target area fraction of that element. Being S_{Co} and S_{Zn} the sputter yields of cobalt and zinc respectively, we can write the nominal cobalt concentration as follows:

$$[Co] = \frac{N_{Co\ sputtered\ atoms}}{N_{(Co+zn)\ sputtered\ atoms}} = \frac{S_{Co}.A_{Co}}{(S_{Co}.A_{Co}+S_{Zn}.A_{Zn})} \rightarrow [Co] = \frac{1}{1+\frac{S_{Zn}A_{Zn}}{S_{Co}A_{Co}}} \qquad (1)$$

Where A_{Zn}, A_{Co} are the target area fraction occupied by zinc and cobalt respectively. Knowing the values of each material area fraction and their sputter yield, in the range of argon ions energy, the nominal cobalt concentration and standard deviation according to the number of strips is:

Table 1 Percentage of cobalt substitution calculated from the number of cobalt strips and covered area at the target surface

# of Co strips	% of Covered area	% [Co]
1	2.3	0.58 ± 0.06
2	4.6	1.2 ± 0.1
3	6.9	1.8 ± 0.2
4	9.2	2.5 ± 0.3

It is important to remember that, after oxidation the molar concentration of cobalt is changed because the oxygen is added. Before thermal treatment we have: $Co_x Zn_{1-x}$, where x is commonly named substitution percentage. After complete oxidation, one oxygen atom is present ($Co_x Zn_{1-x}O$) and the atomic concentration of Co is half of that expressed in the table above. This fact is relevant, since most characterization and quantification techniques can only estimate the total atomic concentration, as we will see in the results section.

3.2 Samples characterization

To understand the sputtering process and the thin film formation, all samples were studied by Atomic Force Microscopy (AFM), X-Ray Diffraction (XRD), current Vs potential curves (I-V curves) and scanning electron microscopy (SEM). The influence of doping and cobalt concentration in gas sensing response was analyzed in terms of XPS, XANES, Raman, and UV-Vis absorption spectroscopies. Below there is a brief outline description of each technique and equipment used.

X-ray diffraction

To characterize the thin film crystalline structure and to reduce the substrate contribution, grazing incidence X-ray diffraction (GIXRD) was performed. It is used a Multi purpose Rigaku Ultima IV x-ray diffraction system with a grazing incidence angle of 1.5º and a source wavelength of 1.54Å (CuKα). The recording of the diffraction patterns was made with a 0.02º step and a dwell time of 5s per point. The XDR patterns were compared with the pattern reported in crystallographic database ICSD (Inorganic Crystal Structure Database), PDF number 01-071-3764 4-831for metallic zinc and PDF #01-079-0205 36-1451 for ZnO (Wurtzite).

Scanning electron microscopy

The SEM images presented in this work were acquired in two types of equipment: An INSPECT F50 Scanning Electron Microscope (FEI, The Netherlands) with a field emission source in the Electronic Microscopy Laboratory from the Research Support Nucleus in Advance Materials NAP-MA-USP) and the Magellan 400 L High-Resolution Microscope (FEI, The Netherlands) in the Structural Characterization Laboratory (LCE-UFSCar).

The beam energy was varied between 2 and 5 keV depending on samples. The samples were mounted in an aluminum stub using double-sided conductive carbon tape. Due to the semiconducting properties of the samples, no conductive coating was necessary. For measurements of structure size and image processing, was used *Image J software*. In circa of 200 particles per image were measure to obtain the particle size mean value.

Atomic force microscopy

AFM measurements were performed in a FlexAFM (Nanosurf Switzerland) with a C3000 24-bit controller and a cantilever TAP190Al from Budget Sensors with resonant frequency 190 kHz. For film thickness determination, it was necessary to remove part of the film by scratching the sample surface. It was assured that the scratching material is not hard enough to scratch the silicon but only remove the ZnO film completely as shown in the figure bellow. The thickness was determined by comparing the height difference between the films and the silicon substrate.
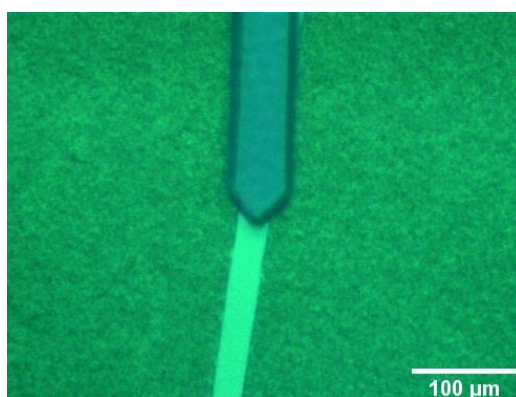
Figure 6 Top view of scratched films for atomic force microscope. Source: by the author.

X-ray photoelectron spectroscopy

To confirm the presence of cobalt at the samples surface, high-resolution XPS measurements were carried out. The spectra acquisition is made in a *Scienta Omicron ESCA +* Spectrometer system equipped with an *EA 125 hemispherical* analyzer and a *Xm 1000*

monochromated, x-ray source *Al kα* (1486.7 eV). The x-ray source was used with a power of 280W and a constant pass energy mode of 50 eV.

The data analysis was accomplished by *CasaXPS* software (version 2.3.16) [45], where the background in high-resolution spectra is computed by Shirley function and charge effect effects were corrected using the 1s carbon peak at 284.6 eV from the adventitious carbon in samples surface.

X-Ray Absorption Spectroscopy

To understand the dopant role in the zinc oxide Wurtzite structure, it was necessary to study the electronic structure of cobalt by X-ray Absorption Near Edge Structure (XANES) spectroscopy. The measurements were performed at the XAFS2 line at the Brazilian Synchrotron Light Laboratory (LNLS), with the storage ring operating between 160 and 220 mA. The spectra were collected with a germanium solid-state detector (Ge-15) 11 channels at the absorption Cobalt K edge (7709 eV) in the fluorescence mode and in the range from 7620 to 7800eV.

For analysis of the XANES data, the spectra were first reduced to a suitable form for interpretation, i.e. by removal of pre-edge background and normalization of the edge jump to one. All the spectra were treated in *Cherokee* software (version 2.5) [46].

UV-Vis absorption spectroscopy

The energy band gap of some semiconductor materials (direct band gap materials) can be optically measured via UV-Vis spectroscopy. This technique stands on the basis that light absorption occurs because of inter-band electronic transitions and hence the absorption energy threshold contains information of the materials band gap.

To obtain the films absorbance as function of the wavelength it was used an Agilent Cary 60 UV-Vis spectrophotometer operating in a wavelength range between 330 and 620nm with a 1nm step and acquisition time of 0.1 seconds per point. Since this spectroscopy is done by transmitted light the films were deposited on glass slides. A blank glass slide was used to monitor glass absorption and to obtain the background spectrum, which was subtracted from all samples spectra.

Band Gap calculation.

The absorption spectra or the absorption coefficient Vs photon energy (α vs E), can be obtained from the collected data (Absorbance vs wavelength) using the equations:

$$\alpha = \frac{Absorbance}{sample\ thickness} * 2.303 \quad \text{and} \quad E = hc/\lambda \quad (2)$$

Where: h, c and λ are plank constant, speed of light and wavelength respectively. For correct determination of the band gap energy, it is necessary to use the equation for the absorption coefficient (α) with the material's band gap (E_g) and photon energy:

$$\alpha = A\frac{(hv-E_g)^n}{hv} \quad (3)$$

Being A a constant independent of wavelength, n equal to $1/2$ for direct band gap materials, and using the α vs E from the experimental data, it is possible to determinate the band gap value from a plot of $(\alpha hv)^2$ as function of hv. From the expression $(\alpha hv)^2 = C(hv - E_g)$ it is easy to note that E_g corresponds to the abscissa intersection of the extrapolated straight-line part of the curve (see Figure 25 at section 4.1.5).

I-V Curves and resistivity calculation

An essential part of studying the electrical behavior of thin films is the behavior of current vs. potential curves (also called I-V curves). For this purpose, the films were deposited on the same platinum interdigitated electrodes used for gas sensing measurements (see Figure 7 and gas sensing measurement section). Using a micromanipulator and a Keithley electrometer, a voltage between -2 and 2 Volts was applied on electrode extremes while measuring the current flowing through the thin films.

For ohmic materials, the relation between voltage and current is linear ($V = i.R$), therefore the material resistance corresponds to the slope of the I-V curve. For resistivity calculation, it is necessary to assume that all films and electrodes fingers are homogeneous and equals. Thus, as the electrode is composed of 14 trails, the measured electrical resistance can be approached as the equivalent resistance of 14 parallel resistors with cross-section area A, length L and resistivity ρ (See Figure 7)

$$R_{eq} = \frac{R_{each\ finger}}{14} \quad (4)$$

where each finger is assumed to behave as an ohmic resistor, which resistance can be expressed classically:

$$R_{each\ finger} = \frac{\rho L}{A} \quad (5)$$

The geometric parameters w and L can be directly measured on the electrodes, with values equal to $w = 4 \times 10^{-3}m$ and $L = 3 \times 10^{-5}m$, while the film thickness (h) is measured

directly from cross-section SEM images and AFM measurements. Therefore, the resistivity of ZnO is computed rearranging the equation above:

$$\rho = 14.R_{eq}\frac{wh}{L} \qquad (6)$$
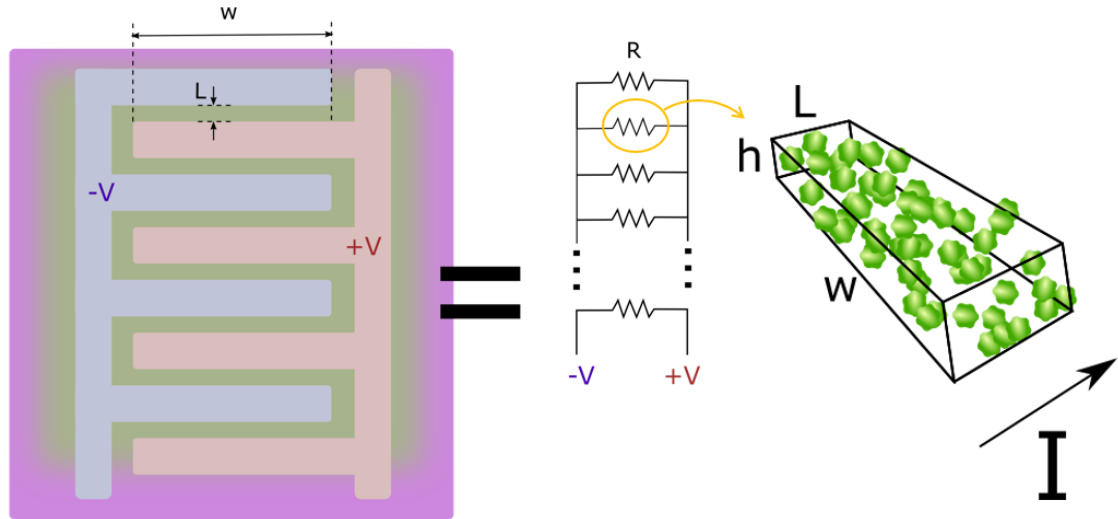
Figure 7 Scheme of interdigitated electrode fingers (left) and circuit approximation used for resistivity calculation (right). Source: by the author.

Raman spectroscopy

To confirm the crystallinity and study the structure of ZnO as well as to understand the effect of Co in the ZnO lattice, Raman spectroscopy was performed directly on gas sensors. It was used an Alpha 300 R Raman Microscope (WITec, Germany) equipped with a 532nm laser. The spectra were acquired using a diffraction grating of 1800 lines per mm with 30 accumulations in 5s integration. The spectra were processed with WITec Project software to remove background and cosmic rays spark lines. Since the film is around 100 nm thick, the signal is weak and increasing integration time and/or number of accumulations did not increase significantly signal to noise ratio.

3.3 Gas sensing measurements

In the brief outline presented in section 2.1, it is not mentioned the importance of aspects as the film-electrode contact, Schottky barrier, the dynamic changes at the depletion layer and the temperature effects. In order to neglect these effects and separate the morphology influence, it is proposed the study of films in the same type of electrode contacts and working temperatures.

To build the gas sensor, the ZnO films were deposited on interdigitated platinum electrodes printed in silica (SiO_2/Si substrates). The fingers are 100 nm thick and spaced by 30μm. The interdigitated electrodes were fabricated by sputtering and photolithography techniques in the Microfabrication Laboratory (LMF) at the Brazilian Synchrotron Light Laboratory (LNLS).

The film deposition is performed directly above electrodes, always depositing the same amount of material (controlled by the quartz crystal microbalance), and generating films of thickness between 96 and 190nm depending on their porosity.
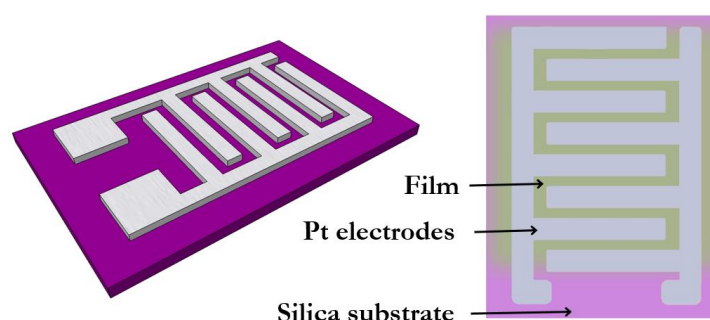
Figure 8 Scheme of printed interdigitated electrodes and films. Source: by the author.

For ozone detection measurements, the sensor is placed on a heating plate inside a sealed chamber equipped with a gas inlet right above the sensor surface (Figure 9). Using two needles of gold coated tungsten on electrode extremes, a constant voltage of 1V is applied while the electrical resistance of the film is measured using a Keithley electrometer (Figure 9). The study of the gas sensing behavior is made by measuring the changes in film resistance in presence of different ozone concentrations and exposure times.
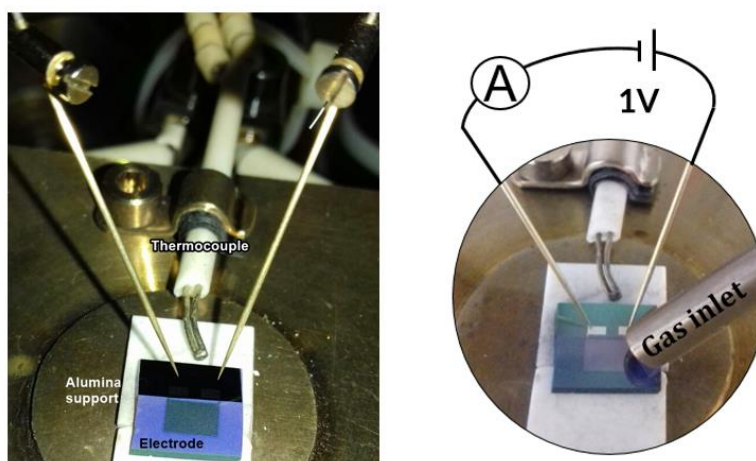
Figure 9 Sensor inside of the measurement chamber. Source: by the author.

As state by the world health organization, the maximum concentration of ozone to which a person can be exposed for 8 hours is equivalent to 0.05ppm of O_3 [11]. Accordingly, the ozone is produced with a pen-ray UV lamp that generates ozone concentrations between 0.05 and 0.89ppm. While the temperature is controlled, a mixture of dry air and ozone is injected right above the sample at a constant flux of 500ml/min. The base line is acquired when injecting dry air without ozone at 0ppm of O_3.

The sensor response is defined as the ratio between the electrical resistance in the presence of ozone and the base line resistance (prior to ozone injection). The response time is defined as the time necessary to the sensor to reach the 90% of the final electric resistance after ozone exposure, while recovery time is the time the sensor takes to return to a resistance 10% above the one before exposure.

4.   RESULTS AND DISCUSSION

4.1 Production of ZnO films and growth conditions influence

4.1.1   Sputtering of metallic zinc target and thermal oxidation

Zn films were sputtered using different deposition powers on silicon substrates The GIXRD data (Figure 10a) shows that, despite the different powers (from 30 to 250W), all films diffraction patterns contain three peaks corresponding to (002), (100) and (101) planes of metallic zinc hexagonal structure.
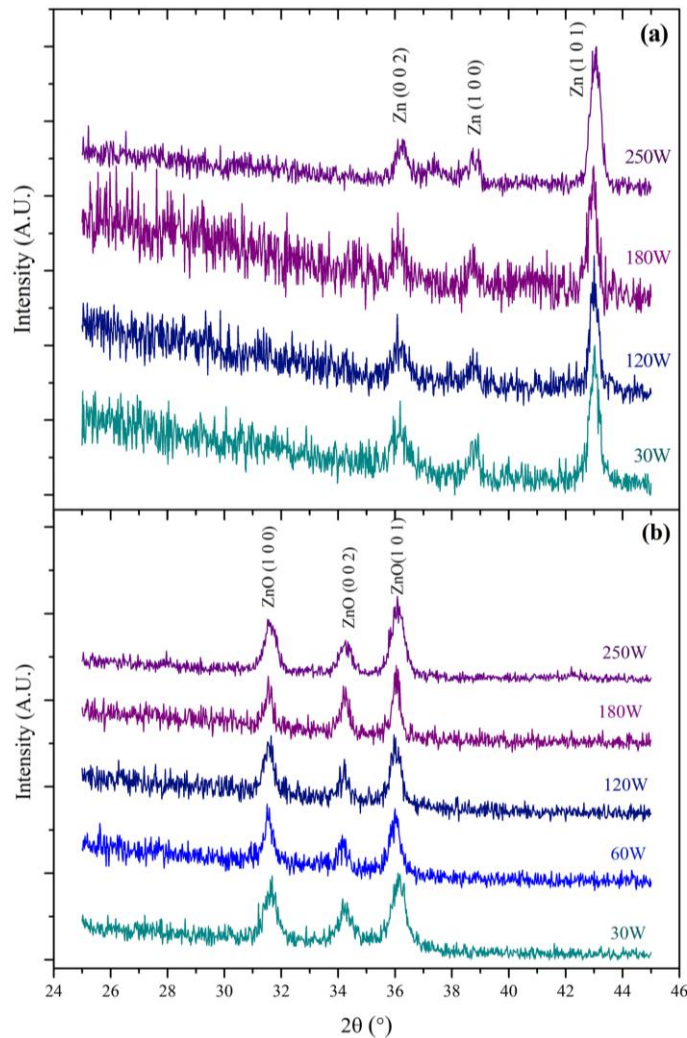
Figure 10 Grazing incidence x-ray diffraction patterns of films deposited on silicon with different sputtering power. (a) As deposited, metallic Zinc exhibits the (002), (100) and (101) planes of hexagonal structure.). The change in crystalline structure is evident in (b), where the peaks evidence complete oxidation of Zn into ZnO (wurtzite). (b) figure shows the XRD patters of films after thermal treatment TT5 (530ºC by 1 hours). Source: by the author.

In order to obtain the ceramic films the zinc films were submitted to different thermal treatments compiled in Table 2. The crystal structures of treated samples are summarized in Table 2 based on the XRD results (data not shown). Not every thermal treatment was equally adequate to achieve the complete oxidation of zinc. The films deposited with the highest powers (180 and 250W), do not oxidize when lowest temperatures and the shortest times of thermal treatments were used.

Table 2 Thermal treatments and their effect in crystal of Zn films.

| Time (Hours)	Temperature (ºC)	Name	Crystalline structure according to the XRD pattern				
			Zn30W	Zn60W	Zn120W	Zn180W	Zn250W
1	380	TT0	Wurtzite	Wurtzite	Wurtzite	Wurtzite + Metallic Zinc	Wurtzite + Metallic Zinc
1	420	TT1	Wurtzite	Wurtzite	Wurtzite	Wurtzite + Zinc hydroxide	Wurtzite + Zinc hydroxide
1	530	TT5	Wurtzite	Wurtzite	Wurtzite	Wurtzite	Wurtzite
0.25	530	TS5	Wurtzite	Wurtzite	Wurtzite	Wurtzite + Zinc hydroxide	Wurtzite

To illustrate, we present the case of Zn250W sample (Zinc deposited with 250W of power) is exhibited in Figure 11. In addition to the expected zinc oxide phase, the XRD patterns of samples with TT1 and TT0 treatments present peaks corresponding to metallic zinc and zinc hydroxide

The only treatment that satisfy the complete oxidation to all the samples was TT5, where samples were submitted to 530ºC during an hour. As shown in Figure 10(b), the diffraction patterns of this oxidized samples, exhibit peaks around 31.6º, 34.2º and 36.0º, corresponding to of (100), (002) and (101) planes according with the standard patterns of zinc oxide compact hexagonal structure (Wurtzite phase). Therefore, this temperature was chosen to carry on all thermal oxidations in this project.
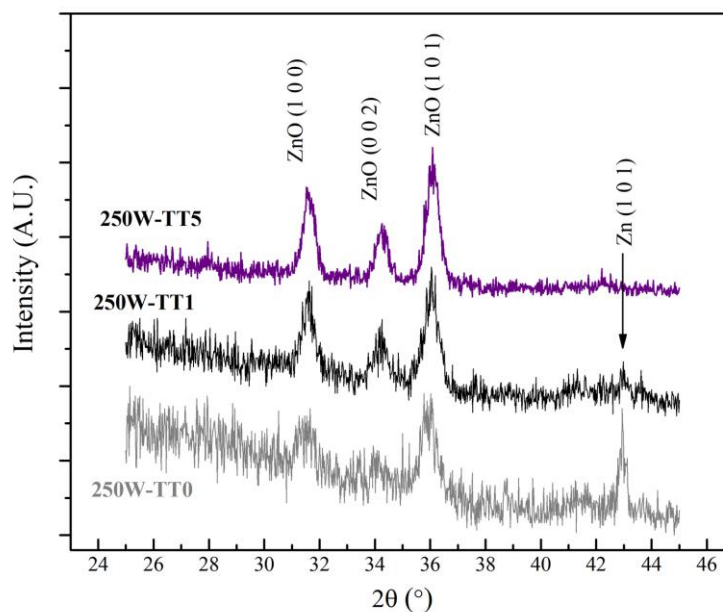
Figure 11 XRD patterns of Zn samples produced with 250W deposition power and oxidized with different thermal treatments. The treatment TT5 is the only to produce complete oxidation on the sample deposited with 250W. Source: by the author.

According to the SEM images, all the films obtained by sputtering of metallic target with deposition powers between 30W and 250W are distinctively porous. Both, metallic and oxidized films (with the TT5 treatment) assumed porous and branched morphologies with structures that reach hundreds of nanometers, as showed in the cross section image of zinc film deposited with 250W on Figure 12.
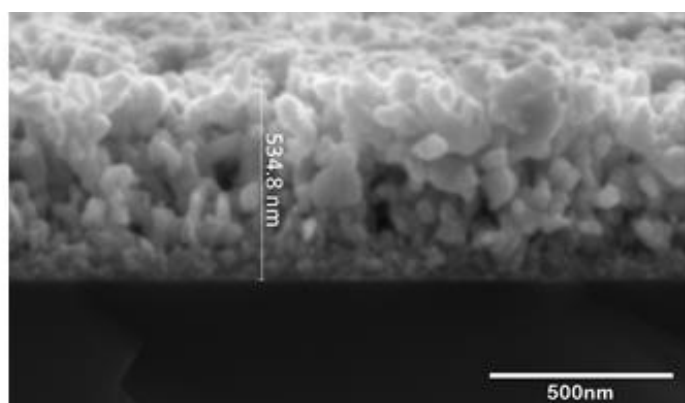

Figure 12 SEM cross section image for Zinc film deposited with 250W deposition power. Source: by the author.

A technical observation must be made before we continue. Even though when the

amount of material deposited is kept constant (using the quartz crystal microbalance), the film thickness is not the same for all deposition powers. As shown below each deposition powers would bring different structure formation porosity, thus resulting in different final thickness. Using Atomic Force Microscopy, the films thickness was determinate with values variating around 530 nm.

Although the films are porous despite of deposition power, the top view SEM images presented in Figure 13 reveal important differences in the structures sizes. It can be noticed that bigger structures result from higher deposition powers. Moreover, it is evident the structures grow when the zinc is oxidized. Using the software ImageJ, the mean feature size[1] was measured, and the real quantitative difference between the structures in metallic and oxidized samples is obtained and displayed in Figure 14.
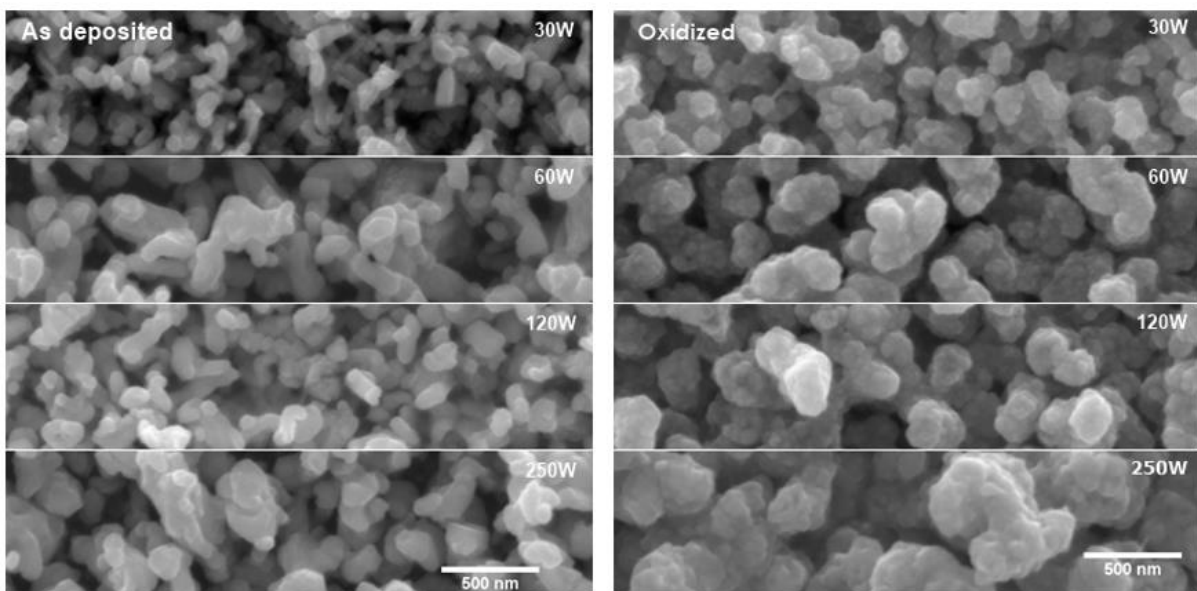

Figure 13 Top view SEM images for metallic and oxidized films deposited in silicon with different deposition powers. Source: by the author.

Even the difference in mean size in not so remarkable for metallic samples, there is a change in the feature size, higher powers tends increase the size dispersion of such structures. The influence of power on the mean feature size of metallic films can be explained considering the sputtering process and the film growth dynamics.

---

[1] We have opted to call it mean feature size rather than grain size or particle size, since these structures are not formed by a single grain or particle. Although this term is not a strict definition in Material Science, it reflects the behavior observed in our sets of samples. Therefore, we are consciously avoiding the terms grain, crystallite and particle in this section.
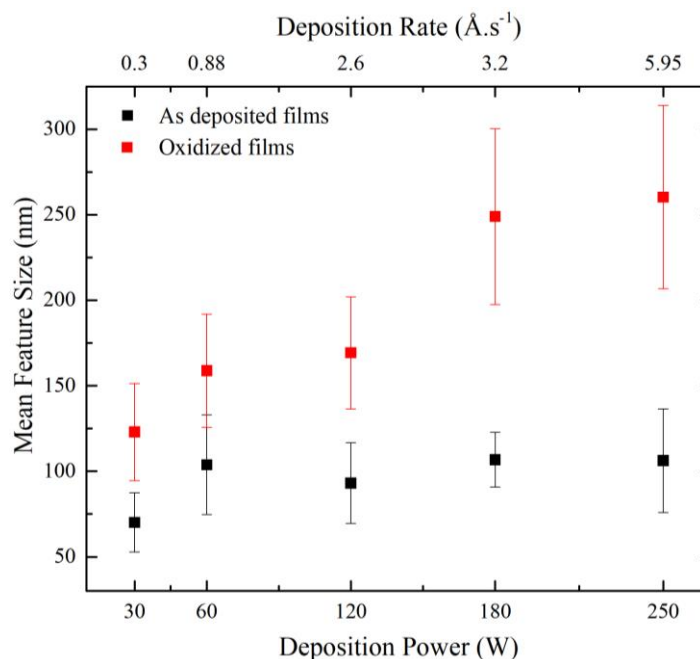
Figure 14 Mean feature size for metallic and oxidized films in function of the sputtering power and respective deposition rate. Source: by the author.

In a RF sputtering system, the deposition power is directly related to the argon ionization potential, this means higher the power higher the concentration of ionized argon atoms, and most importantly, higher the kinetic energy of the ions impinging the target surface. In other words, changes in power indirectly bring changes to the deposition rate and, in less proportion, the sputtered atom velocity; these factors influence greatly the thin film growth. The top axis of Figure 14 shows the deposition rate measured directly from the quartz crystal microbalance.

When ions velocity is high (high deposition power), the number of atoms ejected from the target per each incident atom (the sputter yield) increase, which allows the removal of atoms clusters instead of individual ones [47]. Thus, higher deposition rates lead to the bigger atoms clusters to reach the substrate continuously, giving not time for surface diffusion and organization.

On the other hand, low deposition powers, produce extraction of smaller zinc atomic clusters (or even individual atoms) with lower energies. The deposition rate is low enough for allow the small clusters and/or atoms to form compact structures (less porous structures) and minimize the material energy before the next layer of material arrives.

The feature size of "as deposited" films also affects size of the final structures after oxidation (Figure 14), were the zinc oxide size is proportional to its original metallic structures, observing the initial size of zinc metallic nanostructures have a major influence on ZnO

structures sizes. The influence deposition power on feature size can also be associated with the results of crystalline structure and thermal treatments shown in the previous section. Samples of higher depositions powers, which produced bigger structures, were only oxidized with the more sever treatment, showing signs of incomplete oxidation when treated with intermediary ones; contrarily to the observe for films with small features (less than 170nm) that were oxidized even with treatments of 15minutes. This could be related with the diffusion energy and time necessary to the oxygen atom to react with the zinc and form ZnO. Bigger structures would, therefore, oxidize more slowly at lower temperatures or need more temperatures to be oxidized in a practical time.

4.1.2   Substrate influence

The varied morphologies that zinc oxide can assumed are mostly generated by the different synthesis methods, however, several studies have shown that even using the same production route, it is possible to obtain very different morphologies due to the substrate conditions. Parameters as temperature, morphology, composition and crystal structure of substrate have an appreciable influence, especially due to the strong surface-film interaction that exist in nanoscaled films [47,48].

To study the type of substrate influence on the ZnO formation, films were deposited on silicon, silica and glass microscope slides, maintaining the pressure, temperature and power. Although the XRD patterns, indicate the formation of the Wurtzite phase, the top view SEM images show distinct film morphologies for each substrate (Figure 15 and Figure 16).

Zinc growth on silica (crystalline) results in structures similar to those observed in silicon wafers. However the different surface energies of these materials cause a change in deposition dynamics (wettability, lateral diffusion, heat transfer) resulting in distinct feature size observed for films on silica substrates (70 nm) compared with the size of structures grown on silicon (106 nm).

The deposition on glass (amorphous material) is shown in Figure 16. As reported for other authors, these particular nanoneedles morphology has only been observed in glass substrates, under specific growth and temperatures conditions [49–51]. As stated before, the first stages of growth deeply affect the final morphology of films, thus the absence of a crystalline order in glass substrate results in quite different structures. These results stablish the crystallinity and surface energy are factors that plays a major role in the morphology of ZnO, along with the deposition parameters.
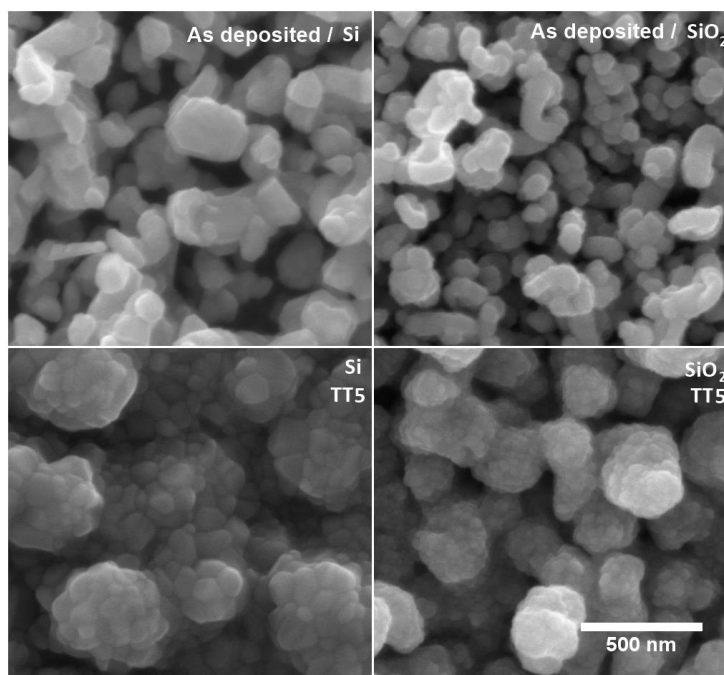
Figure 15 SEM images of sputtered Zn deposited with 250W under same conditions (pressures, temperature and time) in silicon (left) and silica (right) before and after thermal oxidation. The difference in the features sizes can be attributed to the difference in the surface energy of the substrate materials, which changes the deposition dynamics. Source: by the author.
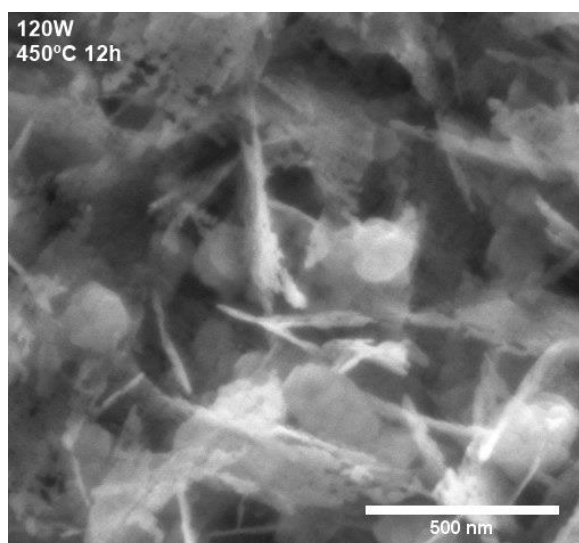

Figure 16 Nano needles of ZnO formed by Zinc sputter deposition (120W) on glass substrates
Source: by the author.
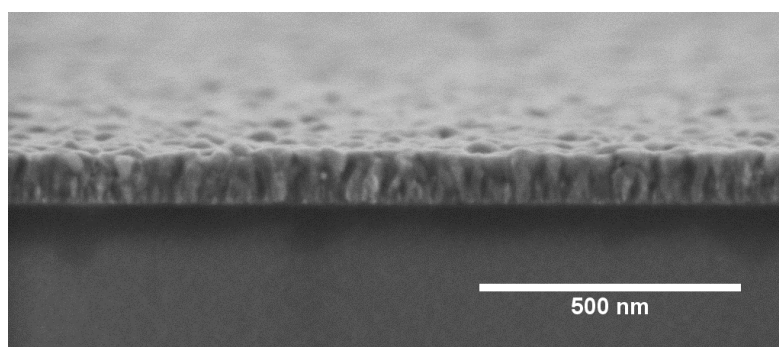
4.1.3 Sputtering of ceramic target (ZnO)

Thin films were obtained from the sputtering of zinc oxide targets using higher deposition powers (150W and 250W). Low deposition powers were impractical due to the very

low deposition rates of ceramic sputtering, (less than 0.1nm/s for 60W). Since the films are already oxidized, no additional thermal treatment was necessary. Thus, the films "as deposited" were investigated by XRD, confirming the formation of zinc oxide with a preferential grown in (002) direction (Figure 17).
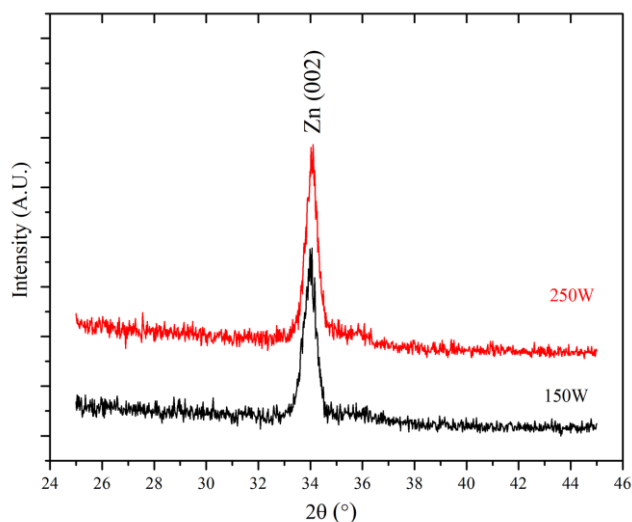
Figure 17 X-ray diffraction patterns of films deposited with ZnO ceramic target**.** Source: by the author.

Besides the preferential growth, there is another critical difference between films obtained from ZnO target to the films obtained from metal one. Films obtained from ceramic target exhibit a greatly compact morphology that highly contrast with the porous films obtained before (see Figure 18).

Figure 18 SEM cross section of ZnO film formed by sputtering of ceramic target. The films obtained this way are more compact than the observed for metallic target sputtering. Source: by the author.

As observed for other ceramic materials, the sputtering of ceramic target always produce compact films due to the low deposition rates [44,52]. This arrange of compact zinc oxide columnar growth has also been observed for reactive sputtering of zinc metallic targets, when the formation of zinc oxide occurs during the deposition process [53].

The top view images of films are presented in Figure 19, showing tightly organized structures similar with nanoslabs. This type of structure and the difference with porous films was also registered by Laurenti et all [54].
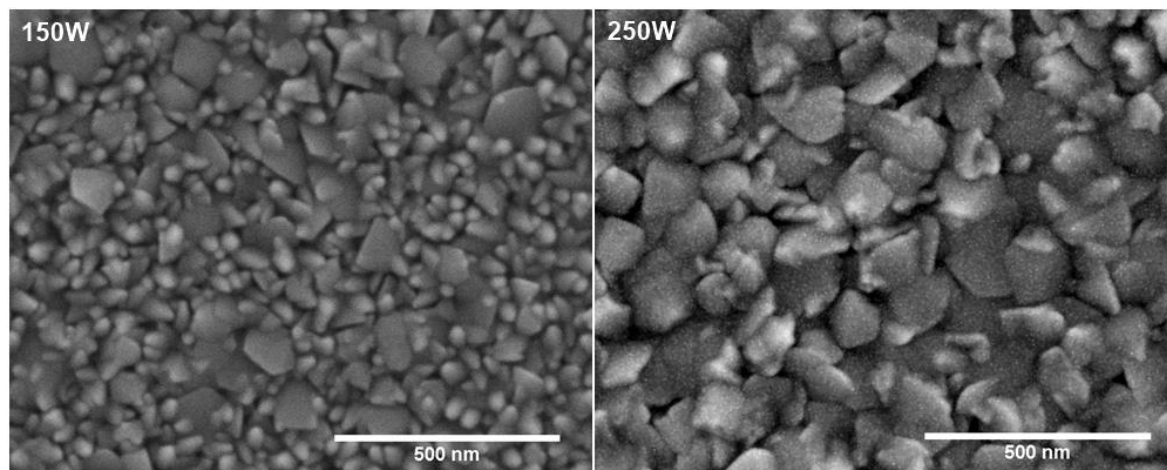
Figure 19 Top view SEM images of films deposited Source: by the author.

From the gas sensing perspective, this type of structures and organized films could present minor benefits. The interaction of these films with gaseous phase would be limited to the geometric surface, which compared with the porous films, will produce lower and limited gas sensibility as we will observed on section 4.2.

4.1.4   Zinc oxide films deposited by sputtering of metal target – response to ozone

Given the influence of deposition power on porosity and morphology of sputtered material, the films for sensor devices were deposited using metallic target and five different powers between 15 and 240W. Parameters as thermal treatment, amount of material deposited and substrate material are kept constant for all sensors. In order to ensure the complete oxidation of films and avoid possible transformations during the gas measurements (involving high temperatures) thermal oxidation is performed with 530ºC during 12 hours.

Before gas sensing measurements, electrodes were chemically characterized by X-ray photoelectron spectroscopy XPS (data not shown). The survey spectra of films before and after thermal oxidation discard the presence of contaminants elements (from the sputtering process) and confirm the metallic and oxidized nature of zinc Zn^{2+}, on metallic and ceramic samples.

To find the optimum working temperature, the films response to 0.13 ppm of ozone was verified at 200, 250, 300 and 350ºC (Figure 20). The response at lower temperatures are not

shown here due to the instability of the signal and low response presented. All the sensors demonstrated to have a maximum response at temperatures near to 300ºC, decreasing rapidly for higher temperatures. Therefore, all the subsequent measurements were made at this optimal temperature. Between sets of experiments and different deposition, we have rechecked the sensors response in function of the working temperature and no shifts were observed. To all sensors, the maximum response was generated around 300ºC.
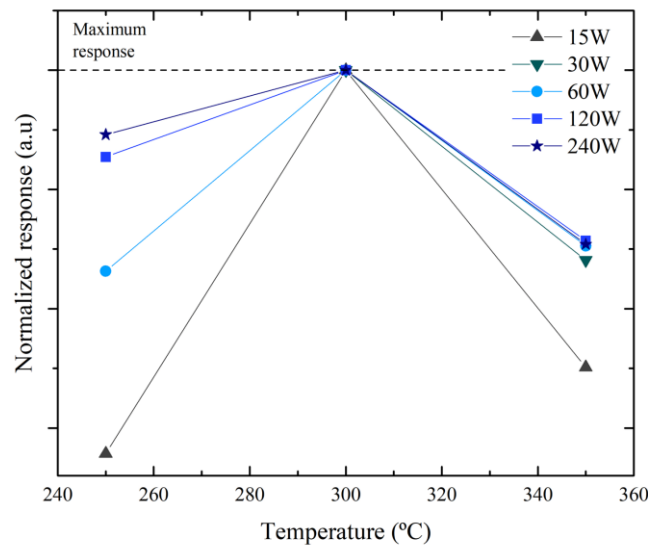
Figure 20 Normalized sensor response in presence of 0.13ppm of ozone on different temperatures. The results are normalized just to illustrate the general behavior of the sensors with respect to the temperature. Once all sensors exhibited the maximum response at 300ºC, it was used as the working temperature for all subsequent experiments. Source: by the author.

The response of sensors to the exposure of 0.13ppm of ozone during 30 seconds is depicted in figure Figure 21. The electric response of all sensors when exposed to ozone behaves as the expected for n-type semiconductors in presence of oxidizing gases, where the adsorption of oxygen at the material surface causes an increase in electrical resistivity. Clearly, the magnitude of the response is strongly dependent on power and deposition rates, which can be explained studying the morphology and structures size of these films.
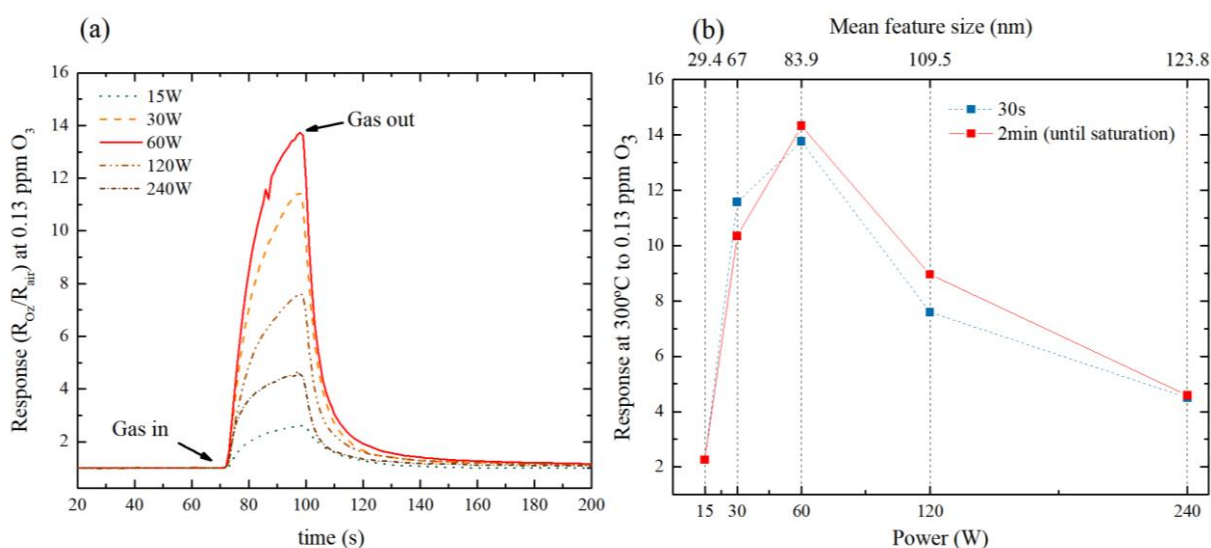
Figure 21 Ozone gas sensing response of ZnO sputtered films, synthetized with different deposition powers (a). Sensors response in function of deposition power and feature size (b). Source: by the author.

From the models used in gas sensing, it is expected that films with larger surface area exhibit greater response. Considering the mean size of the film's structures, it is possible to stablish smaller structures have bigger surface-volume ratio and, consequently, greater response to gas. In order to find this relation on our experimental system, the mean feature size (particles aggregates) of zinc oxide sensors was measured from the top-view SEM images, as done before. On Figure 22 it is possible to observe how the mean feature size evolves as function of the deposition power. The features grows rapidly from 15 to 60W, after which the growth is slower. Figure 22b exhibits the response as a function of feature size. It is the same data of figure21, however it is presented as a function of feature size rather than the deposition power. It can reveal a new insight on the sensing mechanism.

As stated before, the results indicate that higher deposition powers brings bigger ZnO final structures (Figure 22b), with sensors structures that relies in the range between 29nm (for 15W deposition power) and 124nm (240W).

Despite our belief of small features sizes cause high sensor responses, it has been found that this dependence is only valid for deposition powers bigger than 60W with 84nm structure sizes. As presented in Figure 22a, the magnitude of the sensor response rapidly decrease for smaller structures (deposition powers lower than 60W).

At this point, the influence of deposition power on surface area and sensor response can be clarified studying the images of sensors presented in Figure 23. Although the differences in

structure size is evident for all samples in top view images, the cross-section ones highlight an additional difference in films porosity.
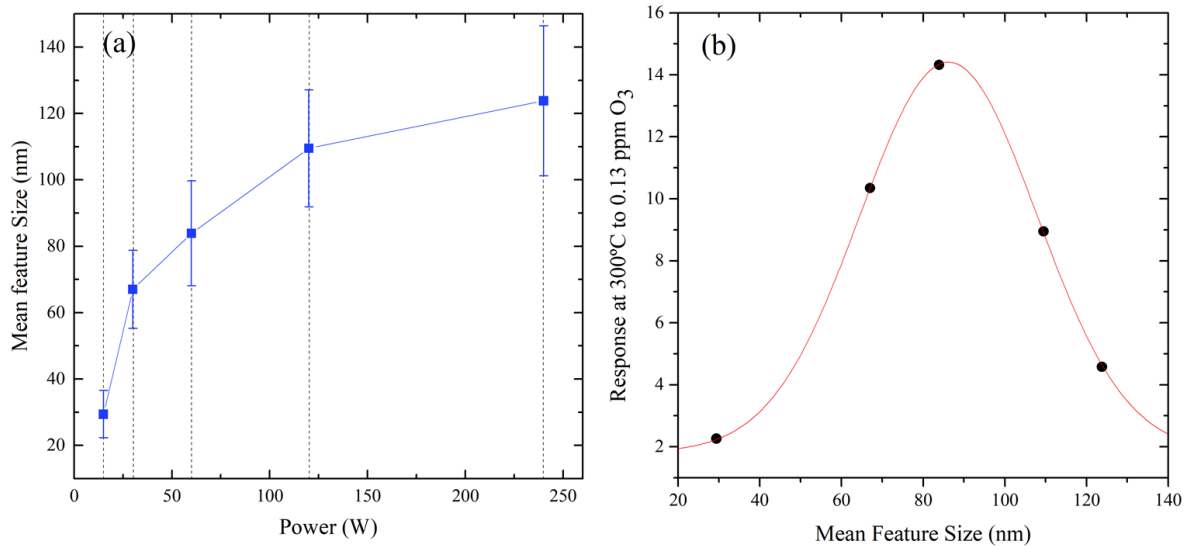
Figure 22 (a) Evolution of mean feature size as a function of the deposition power. (b) Response to ozone vs. mean feature size. The mean feature size of sensors was estimated using the top view SEM images of Figure 23. Source: by the author.

Films with the smallest structures sizes (15W and 30W) present more compact structures than the rest. Here, the small size of features and the low deposition rates, inhibit the formation of porous structures, which can limit the interaction with gaseous phase and restrict the gas sensor response. The opposite is observed in films deposited with higher powers, where the main feature is the great porosity observed in cross section images. In this case, the high deposition rates allow bigger structures to reach the substrate in such rapid way that surface diffusion is not possible and the formation of cavities and "chambers" between particles aggregates is promoted. This aspect enhances the surface area available for gas adsorption allowing the gas to interact with film bulk.

According to these results, it is natural to suppose that the surface area available for gas adsorption is determined by a combination of structure size and film porosity. The results suggest that even tough a small size of structure imply a bigger surface-to-volume ratio, porosity is so low that the surface available to adsorption is small, as well as the film response. On the other extreme, although the highest deposition rates produce highly porous films, very large structures can reduce the surface-to-volume ratio of aggregates, which also diminish the surface area for adsorption. Apparently the sensor that reunites the best combination of porosity and structure sizes is the film deposited with 60W (features size 84nm).
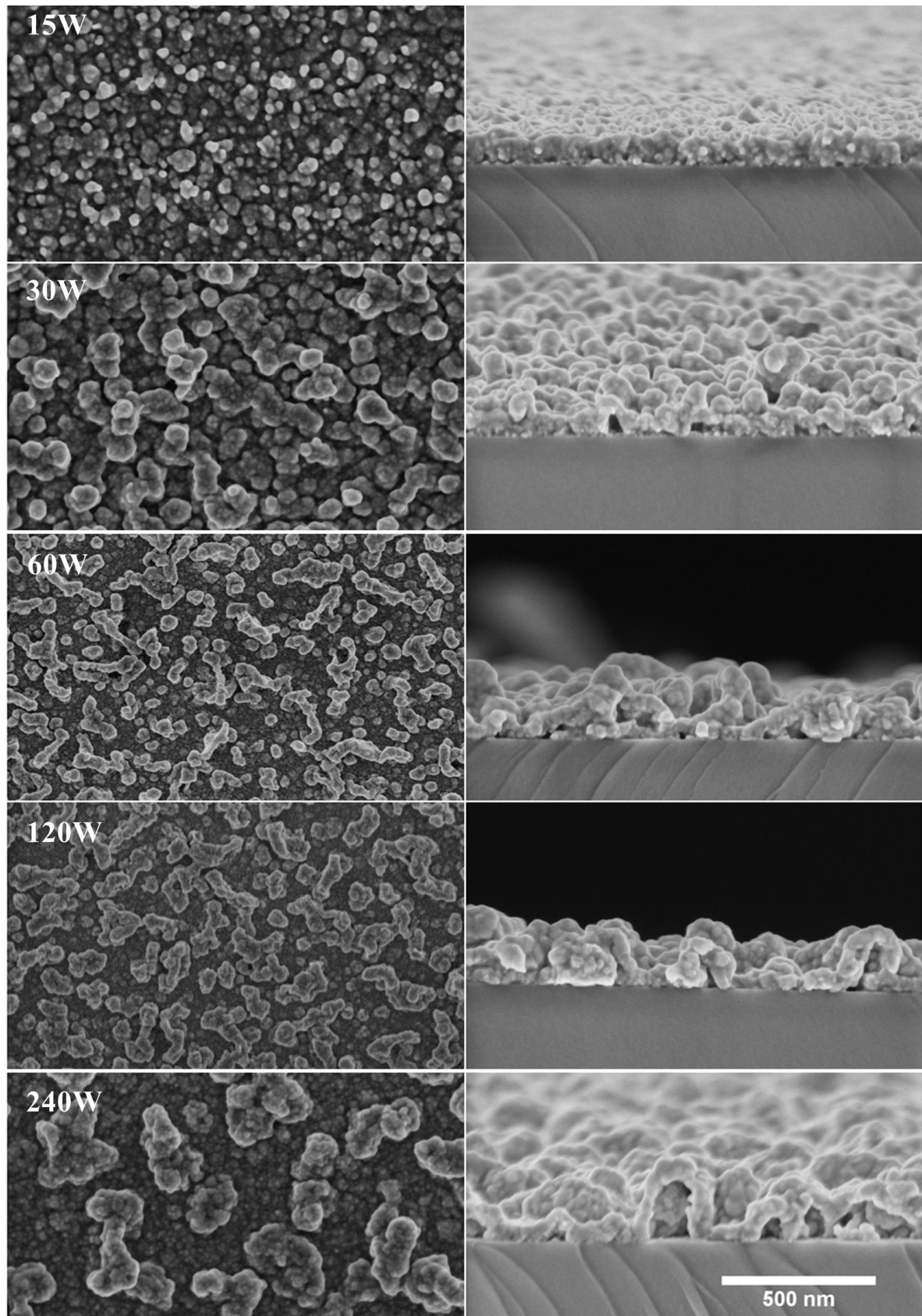
Figure 23 Top view (left) and cross section (right) scaning electron microscopy images of sensors . It is noticeable the changes in the sizes of the features as well as in the porosity as the deposition power increases. Source: by the author.

4.1.5 Electronic structure and resistivity in function of deposition power

A possibility that must be considered and that could potentially explain the differences in sensor response is the probability of we are dealing different types of ZnO semiconductors. Even when the deposition method and thermal treatment are the same for all samples, the use of different deposition powers could have produced zinc oxide films with differences in the electronic band structure or defects density. Therefore, to avoid misconclusions and be able to affirm that ZnO different responses are caused by the apparent differences in surface area, it is necessary to investigate the electrical properties of the ZnO films.

Current-voltage curves of ZnO films were measured in order to find films resistance. As shown at the inset of Figure 24, all I-V curves, confirm the ohmic contact between the film and the electrode, which allows us to discard the possibility of the type of contact influence on the electrical measurements.
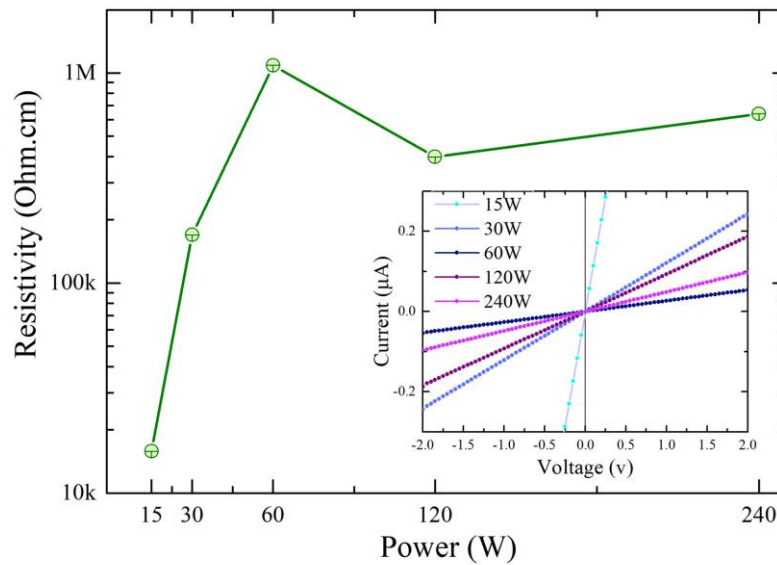

Figure 24 Zinc oxide films resistivity as function of the deposition powers; on the inset the I-V curves (inset) used to obtain the resistivity. Source: by the author.

The resistivity values found for ZnO films ranges between 10^3 and 10^6 Ω*cm, which are consistent with the values reported for ZnO sputtered films. This high values are usually associated with the absence of defects responsible for the conductivity of ZnO matrix (oxygen vacancies) [55,56]. As Figure 24 exhibits, the dependence of films resistivity with deposition power follows the behavior of the sensor response magnitude of Figure 22. The film with the biggest resistivity of 1MΩ is the film deposited with 60W (biggest response), while the small deposition powers generate films with the smallest resistivity values (170kΩ and 15KΩ).

Lu and Wong study [56] affirm that thermal treatment conditions (atmosphere, temperature and time) are factors that influence changes in ZnO resistivity the most. In this case, as the thermal treatment to obtain ZnO films is the same for all powers, we can think the population of ZnO defects is approximately the same for all the samples and that the differences in resistivity comes from the structure sizes and porosity.

The absorbance spectra (Figure 25) allows the calculation of band gap energy. All films results in values around 3.20 eV with irrelevant variations between samples. As reported by Ismail et all [57], this results confirm that sputtering deposition power do not affect the gap energy between valence and conduction bands, whose invariance can attribute the resistivity variations to morphology differences.
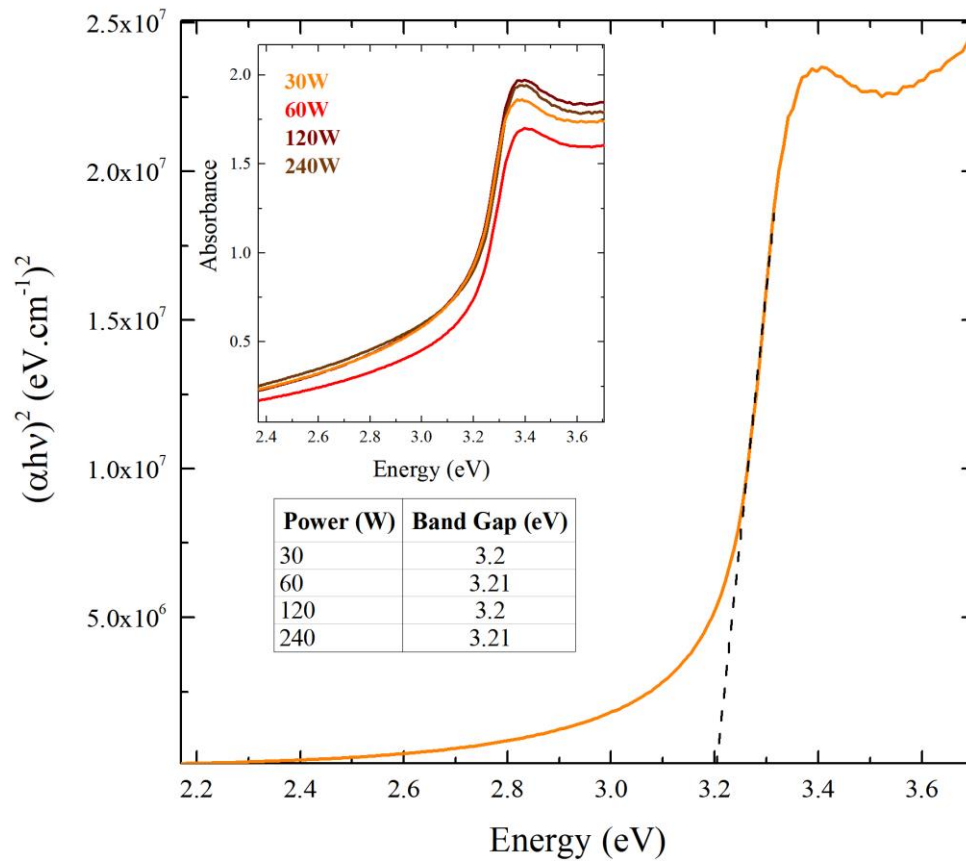
Figure 25 Absorbance spectra of zinc oxide films deposited with different deposition powers (inset) and a demonstration of how band gap values were calculated from the intercept with the energy axis. Source: by the author.

As described in Materials and Methods section, the values of resistivity are computed considering compacts films without pores. In such manner, it is expected that films with small features and considerable high pore volume between structures would present more potential

barriers to limit the current pass. Using this approach to explain the results of films resistivity in function of deposition power (Figure 24), it is noted that indeed, we can directly associate the lowest resistivity (15kΩ) with the most compact film (film deposited with 15W) where the current easily goes through. While increasing the deposition power (until 60W), the volume of the film occupied by pores increase, limiting the current flux and causing and increment of resistivity until a maximum value circa of 1M. For films deposited with 120 and 240W, an opposite tendency is observed and films resistivity starts decreasing until a 58% of the maximum value. Despite of the pores volume increase, there is another factor: the great features facilitate the electron current flow more than the feature size of 60W sensor with smaller structures.

Confirming the absence of differences in composition and electronic structures of sputtered samples, is important to settle that the deposition power appears to affects only the size and morphology of zinc oxide final structures. Since our sensors are chemically indistinguishable, the differences in response magnitude may be completely attributed to the morphologic differences and the amount of surface area that each sensor has available for gas interaction.

4.2 Zinc oxide films deposited by sputtering of ceramic targets – response to ozone

The response to ozone (0.13ppm) of films deposited with ceramic target and deposition powers of 60W, 120W and 240W are shown in Table 3. In order to compare with the results from the previous section, the exposition time was kept in 30 seconds. The sensors showed to have the lowest electrical responses of ZnO sensors obtained in this work; even the sensor deposited from metallic target with the lowest response (15W) presents almost twice the response of these compact/dense films.

Table 3 Sensing response of films deposited with ceramic target after 30 seconds of ozone exposure.

Deposition power (W)	Response (R_{ozone}/R_{air})
60	1.28
120	1.6
240	1.7

According to the conclusions established in the previous section, we can suppose that compact morphologies and faceted surfaces of ceramic targets films (section 4.1.3) restrict the gas access to the sensor bulk, diminishing the number of adsorption sites available and thus the

sensors response.

The dense morphology and preferential growth of ZnO films from ceramic target, also affects the films resistivity. Data of current vs. potential measurements (curves not shown) reveals a characteristic ohmic contact and films resistivity from order of $10^2\Omega.cm$, which contrast with the greater resistivity of porous films (resistivities from 10^4 to 10^6 $\Omega.cm$).
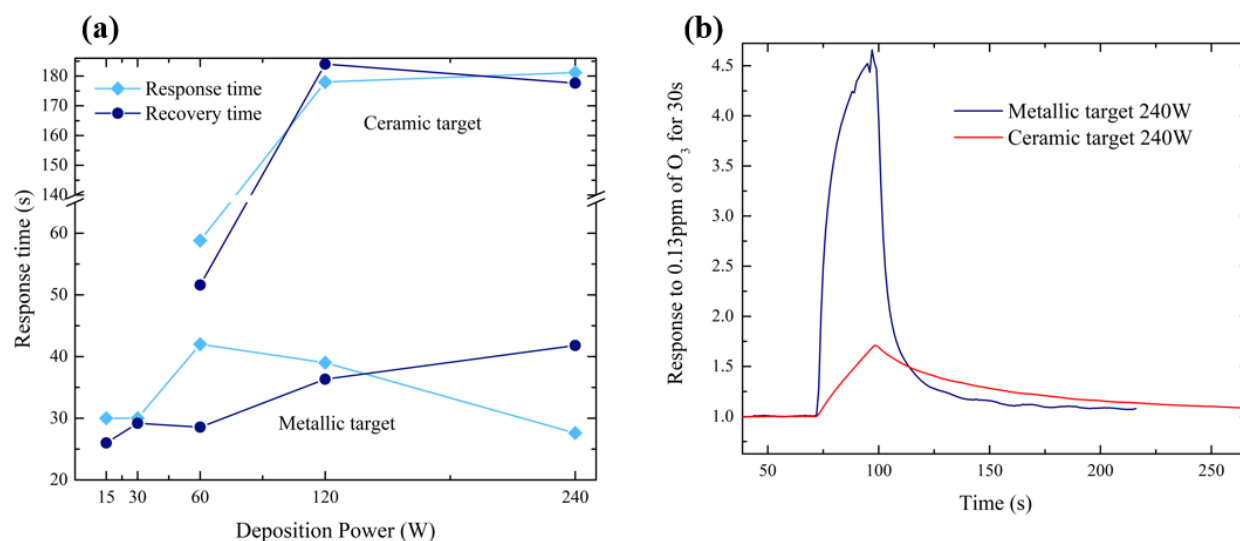
4.2.1 Response and recovery times

In agreement with the current demand for gas sensors to monitor air quality, it is mandatory to develop sensors with short response and recovery times. The principal necessity is to develop sensor with a high response speed, to detect the presence of pollutant gases before it represents an environmental or health threat.

For determination of response and recovery times, all the sensors were exposed to 0.13ppm of ozone until sensor saturation at 300ºC. The sensors characteristic times are showed in Figure 26.

All the zinc oxide sensors produced from metallic target present short responses and recovery times below 42 seconds. The fast response characteristic of this sensor is also observed in **Figure 21**b, where responses after exposure times of 30s and 120s are registered and it is not observed any significant dependence of it with exposure time.

The maximum value of response time is observed for sensor deposited with 60W (mean feature size of 84nm) decreasing for sensors with higher and lower deposition powers. Thinking in terms of the number of absorption sites and surface area, those results are perfectly consistent with the surface area approach presented in this work. The sensor saturation is related to the occupation of all adsorption centers in the ZnO surface. If the we consider that sensors are chemically indistinguishable, as stated before, the density of surface adsorption centers would be the same for any power, and the differences of adsorption sites number would be caused by the distinct surface area. Therefore, sensors with greater surface area will take more time to occupy all the adsorption centers and then will have higher responses times. On the other hand, the sensor deposited with the lowest power (15W) and apparent low porosity have the lowest response time, reaching 90% of its total response after 25 seconds of exposure. The same response time of 25 seconds is measured for the sensor deposited with 240W, which despite of the great porosity, have the greatest structure sizes that decrease the surface area.

Figure 26 (a) Response and recovery time of zinc oxide sensors deposited with metallic (Zn) and ceramic target (ZnO). (b) Gas sensing response of sensors deposited with 240W using metallic and ceramic targets and exposed during 30 seconds to 0.13ppm of ozone. Source: by the author.

The *Langmuir adsorption model* [58] describe the adsorption rate dependence with coverage, surface energetics and order of adsorption. Although the desorption mechanism also depend of those factors, exist other additional parameters that rule the desorption mechanism and explains the difference between response and recovery time behaviors. Factor as the vibrational frequency of adsorbates at the potential well and the probability of oxygen re-adsorption, make difficult to understand the tendency of the curve. Nonetheless, the importance of those results is to confirm the short recovery times all of them below 40 seconds.

As observed in Figure 26, the response and recovery times of ceramic target sensors are considerably greater than the observed for porous films. In spite of the low surface area available for adsorption, the high response times presented by this sensors raises the possibility of gas detection by other than adsorption of oxygen at the sample surface. As exposed in other works, there is a possibility of film-gas interaction through gas diffusion process [3,59,60], which would involve longer times and higher temperatures to make it possible. Even that for comparing purposes it was used the same working temperature of 300ºC for all sensors, is important to add that all sensors from ceramic target, present ozone responses at 350ºC of the same magnitude of responses at 300ºC, which can make us think in the existence of a working temperature bigger than 350ºC. The sensing by contribution of a gas diffusion process would also explains the great recovery times in contrast with the observed for metallic target sensors (see Figure 26b).

4.2.2 Response curve of Zn60W with increasing ozone concentrations

Once the zinc oxide sensor deposited with metallic target and 60W exhibits the highest response, its performance in in crescent ozone concentrations is studied.

The sensor resistivity at different ozone concentrations is shown in Figure 27, where is possible to note there is a variation of the response directly proportional to the gas concentration. The lack of a saturation point in Figure 27 right indicates that the sensor detection limits are likely higher than the values studied here. After exposing sensor to the greatest concentration of target gas (0.89ppm), another exposition to 0.13ppm of ozone is performed. At this exposure, the variation in sensor resistivity is in good agreement with the value observed in the first cycle, which confirm the total recovery of the sensor to his original state and discard the possibility of film degradation or irreversible reactions during the detection process.
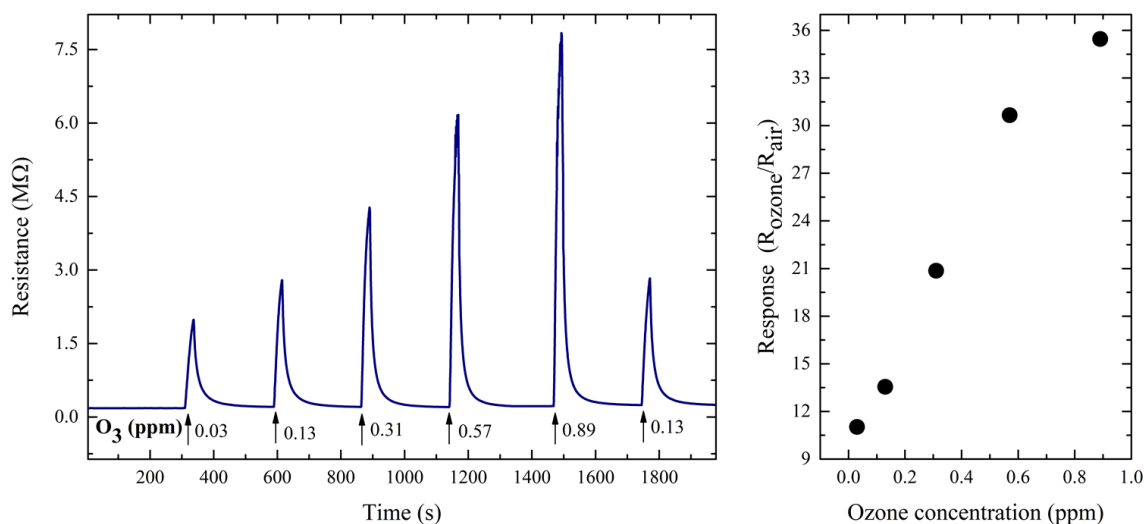
Figure 27 (Left) Electrical resistance of ZnO sensor deposited with a metallic target and 60W. The sensor is exposed at different ozone gas concentrations during 30s with 5 minutes intervals. (Right) Sensor response as function of ozone concentration. Source: by the author.

4.3 Cobalt doped ZnO Sensor

To proceed with cobalt doping, the deposition with 30W is chosen based on the results of the previous sections. All doped samples were deposited by sputtering of metallic zinc and cobalt target in four cobalt concentrations (section 3.1) and with a deposition power of 30W.

4.3.1 Characterization

X-ray diffraction was performed to identify the presence of second crystalline phases

and material segregation. The XRD patterns for all samples exhibit three peaks at 31.6º,34.4º
and 36.2º corresponding to (100), (002) and (101) diffration planes of Wurtzite ZnO structure,
respectively. Despite the low signal to noise ratio, no other crystalline phases wereobserved.
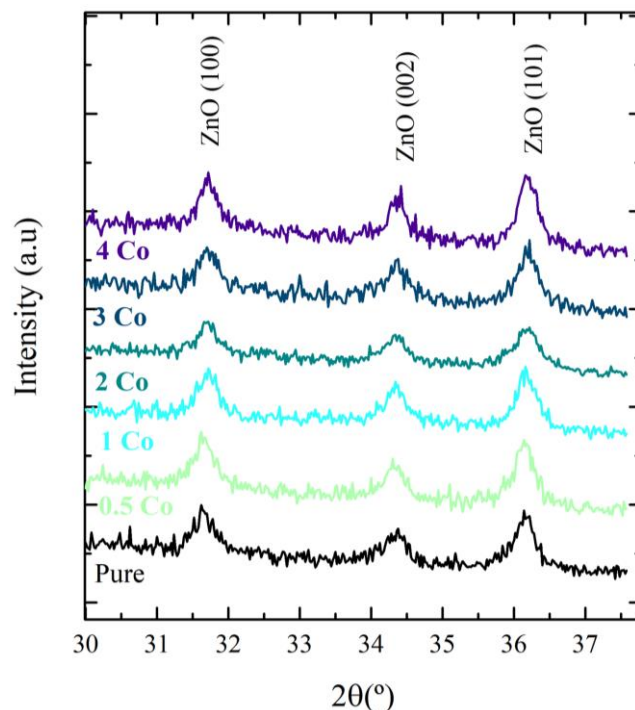
Figure 28 XRD patters of ZnO films doped with four different cobalt concentrations. All the patters
show the formation of ZnO in Wurtzite phase. Source: by the author.

In terms of morphology, the doped films show similar porous structures which sizes lie
around 70nm and similar to those of the pure Zn film deposited with 30W (Figure 29).
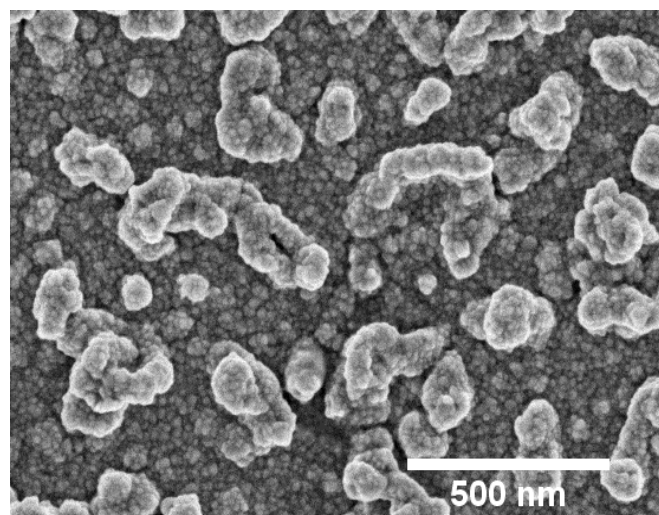
Figure 29 Scanning electron microscopy image of ZnO film doped with cobalt, using 2 strips of cobalt
on zinc sputtering target. Source: by the author.

The confirmation of the cobalt presence at the surface/bulk of the doped samples is
achieved by recording the high-resolution XPS spectra of the cobalt region (775eV-810eV) and

studying the EDX spectra of the films. The measurements reveal the cobalt presence at the compositions specified in Figure 30 as function of the number of cobalt strips placed on the zinc target. The cobalt concentration differs with the technique (XPS and EDX) due to the possible differences in concentration between surface and bulk and, likely, to the limit of quantification of these techniques are close to the concentrations studied..
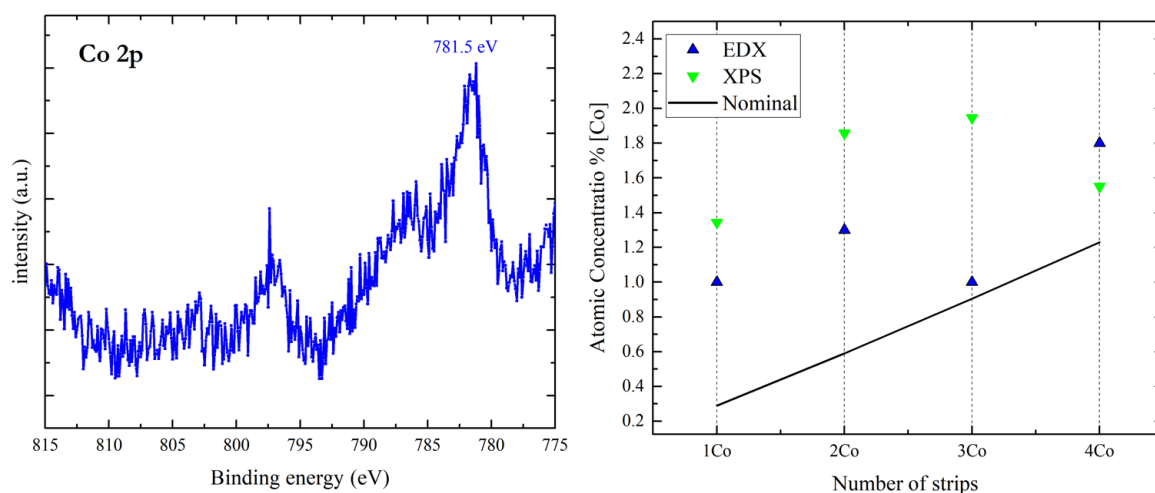

Figure 30 XPS spectrum of cobalt at sample deposited with one cobalt strip (left) and atomic cobalt concentration determined by XPS (▼) and EDX (▲) as well as the nominal concentration (straight line) as function of the number of cobalt strips. Source: by the author.

The X-ray absorption spectra at the pre-edge and edge region of cobalt (7620-7700eV) is studied (Figure 31) to provide information about the cobalt valence state and site symmetries in the ZnO matrix.

The signal to noise ratio increase with the number of cobalt strips and the absorption edge for all samples is determined at 7721.0 eV. This value can be associated with the predominant presence of cobalt in the oxidation state +2 [43, 61],.The information about the local symmetry contained at the pre-edge region (around 7710 eV) is not easily identifiable due to the low content of cobalt in samples 0.5Co, 1Co and 2Co (less than 1.3%). Nevertheless, comparing the shape and intensity of cobalt pre-edge with the structures observed by a previous work from our group (Catto et al. [43]), it is possible to propose the cobalt is at an octahedral and/or tetrahedral site. The reason for such ambiguity is that the pre-edge of our samples are similar to each other and close to the observed for $CoAl_2O_4$ and Co_3O_4 , where cobalt occupies tetrahedral and octahedral/tetrahedral sites respectively. Even though it is not possible to unequivocally determine the site position of cobalt in these compounds, the cobalt at a tetrahedral site fits with the zinc substitution, which occupies a tetrahedral sites at ZnO Wurtzite structure. The pre-edge structure for cobalt oxide (CoO), where cobalt is exclusively occupying

octahedral sites, contrast significantly with the pre-edge of our samples. Thus, we may affirm that the cobalt in our samples are in tetrahedral symmetry or in a mixture of tetrahedral/octahedral sites.
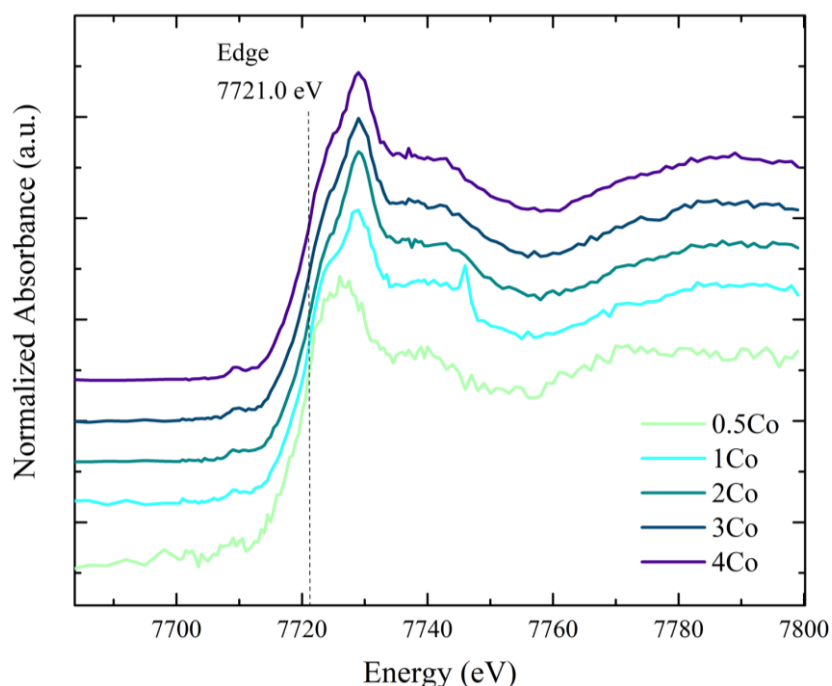
Figure 31 X-ray absorption near edge spectra (XANES) of the K-edge cobalt region, for ZnO samples. doped with different levels of cobalt. The energy edge indicate the cobalt at Co^{+2} state predominantly. Source: by the author.

4.3.2 Response of cobalt doped films to ozone

As pure films, doped films exhibit a maximum response at temperatures around 300ºC. The gas sensing performance of zinc oxide sensors doped with cobalt is studied under the same conditions as ZnO sensor (exposure of 0.13ppm O_3 during 30s at 300ºC).

The electrical responses of doped films are summarized in the Figure 32 and Figure 33, where the semiconductor type changes with the cobalt content. For lower cobalt concentrations, the ZnO sensors present the typical response of an n-type semiconductor in presence of oxidative gases (Figure 32). Indeed, at doping concentrations of 1.3% Co (2strips Co) it is observed an increment in the response in almost 62% compared to the pure zinc oxide response.

On the other hand, increase of cobalt content (3 and 4Co strips) modifies completely the material behavior, and the exposure to ozone causes the decrease of electrical resistance as expected for p-type (Figure 33). The electrical conductivity of these sensors is by means of

positive holes instead of electrons, meaning that oxygen adsorption, which creates positive holes in the conduction band, improve the material conductivity. It is important to note that the magnitude of the electrical response increase with the cobalt concentration, suggesting the p-type semiconductor behavior would increase with the cobalt content.
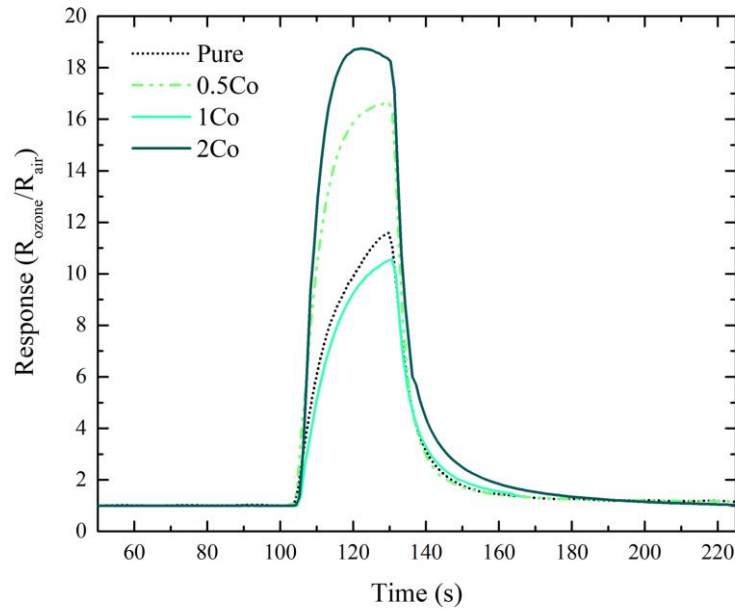
Figure 32 Gas sensing response of sensors doped with 0.5, 1 and 2 strips of cobalt in presence of 0.13ppm of ozone at 300ºC. The sample 2Co represent an increase of sensor response around 62% of the pure zinc oxide under the same conditions. Source: by the author.
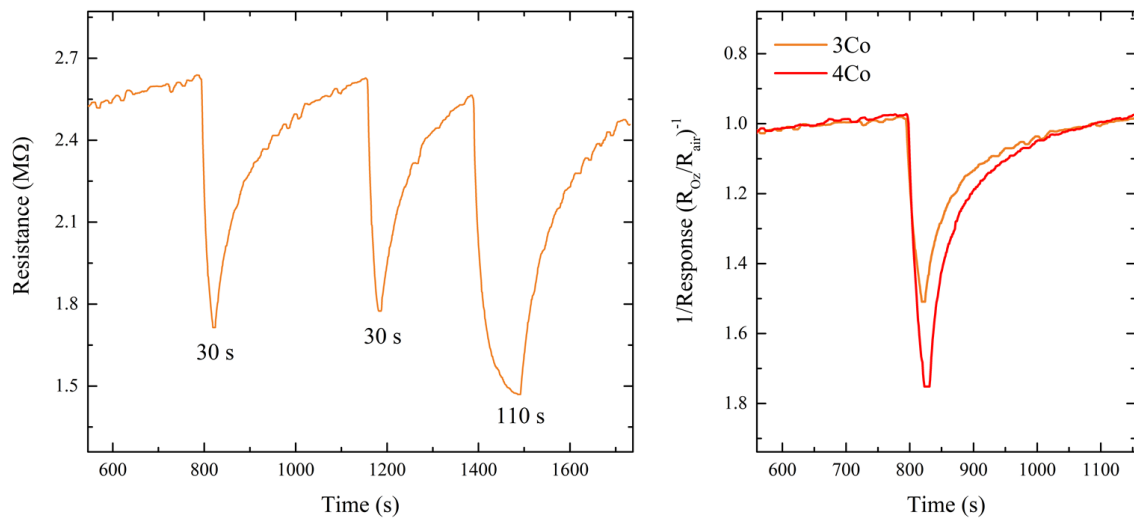
Figure 33 The sensing response of sensors deposited with 3 and 4 cobalt strips present a p-type semiconductor behavior, decreasing the electrical resistivity in presence of ozone. The response of sensor doped with three cobalt strips and exposed to 0.13ppm of ozone during 30, and 110 seconds (left), and the reciprocal sensing response of 3Co and 4Co sensors (right). Note that the response magnitude increases with the cobalt concentration. Source: by the author.

4.3.3 Cobalt influence on the crystal and electronic structure of ZnO

As the cobalt addition is the responsible for the change in type of semiconductor, the doped samples behavior is studied in terms of the chemical composition and electronic structure of samples. To elucidate the cobalt role at the zinc oxide structure and understand the changes introduced with the addition of cobalt, the full width at half maximum (FWHM) of XRD peaks is used to calculate the crystallite sizes of doped samples.
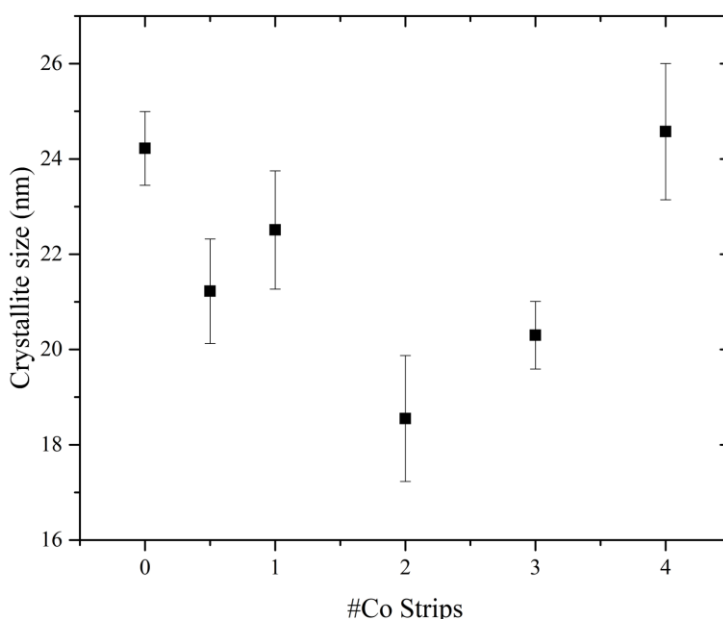
Figure 34 Crystallite sizes of doped samples, computed from the full with half maximum of XRD peaks and using the Scherrer equation. Source: by the author.

Figure 34 shows the crystallite size in function of the number of strips. Clearly the crystallite size decreases moderately with the dopant addition until cobalt concentrations of 0.6% (2 strips of cobalt), where the increment of cobalt content seems to promote the growth of crystallites. As reported for other authors, the decrease tendency in grain size is typically associated to the substitution of Zn^{+2} by dopant atoms, whose introduce a structure asymmetry that limits the crystallite growth [31,33-34,62]. Our results suggest that until 0.6% of cobalt addition, the dopant atom occupies the tetrahedral sites of zinc, decreasing the ZnO crystallite until 18nm.

Since XRD patterns depict the formation of Wurtzite structure indifferently from the cobalt concentration, the increment in mean crystallite size for samples with higher cobalt concentration may indicate the appearance of segregates with bigger crystallite sizes as reported by Alkahlout et al. where they have doped zinc oxide with aluminum [34]. In their study, doping ZnO with aluminum brings a decrease in crystallite size until doping ratios between 0.5 and 2

mol%, above which the crystallite starts to grow. They affirm the increment of dopant presence reach a limit of Al solubility where aluminum oxide occurs as secondary phase.

In an attempt to clarify the chemical state of cobalt at 3Co and 4Co samples the band gap energy and resistivity of films is studied (Figure 35 and Figure 36). When an impurity atom is forming part of a semiconductor material as dopant, it introduces changes in the band gap by introducing additional energy states near the conduction or valence band; indeed, one possibility of doping semiconductors is to decrease the band gap energy between bands and thus enhance the material conductivity.

As presented in Figure 35, increasing the dopant level in zinc oxide samples effectively decrease the material band gap until atomic cobalt concentrations of 1% (3 Co strips), which is in agreement with the observed for other authors when ZnO is doped with materials as Al, Mg and even Cobalt [33,63]. Nevertheless, the opposite happens when cobalt concentration increase to *circa* of 1.2% (4 cobalt strips), where there is a considerable increase in band gap.
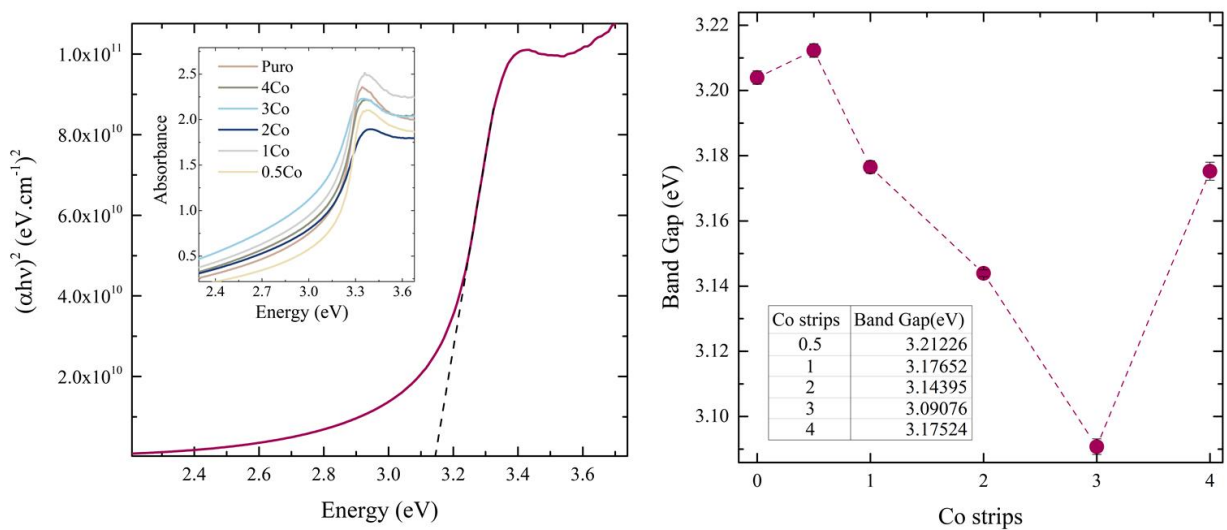
Figure 35 Absorbance spectra of doped zinc oxide films and a demonstration of how band gap values were calculated from the intercept with the energy axis (left). Band Gap energy as function of the number of cobalt strips used for sputtering doping. Source: by the author.

The same tendency is observed for the resistivity values of doped films in Figure 36. Until 1% of cobalt concentration, the dopant addition decreases the material resistivity tenfold, while doping at 1.2%Co (4 strips) rapidly increase the resistivity to 10^6 MΩ*cm. This behavior was also reported by the paper of Li et al when increasing the magnesium doping in ZnO [63]. In their work, the increase of dopant level not only rises the values of material band gap and resistivity but transforms the semiconductor behavior from n-type zinc oxide to p-type zinc oxide, concluding that conduction type of ZnO would depend on the Mg content. Li et al explain

the rise in band gap as a consequence of magnesium segregation, where energy band gap for ternary semiconductors is a combination of band gap of both components (The principal and segregate phases) and the growth of magnesium oxide aggregates increase the band gap values.
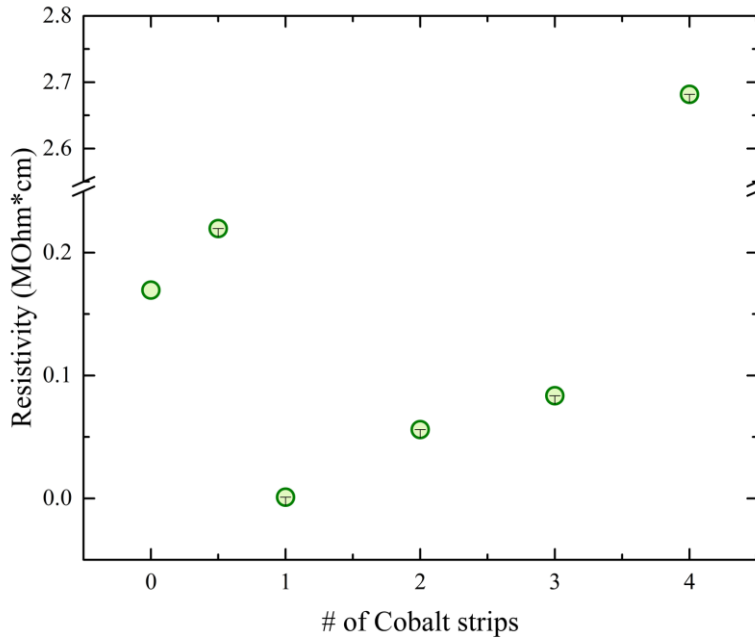
Figure 36 Electrical resistivity of doped samples as function of the cobalt strips used for doping. Until 1% of cobalt concentration, the dopant addition decrease the material resistivity from 10^5 to 10^4 MΩ, while doping with four cobalt strips rapidly increase the resistivity to 10^6 MΩ*cm. Source: by the author.

The paper presented by Belkacem et al. [16] reveals the effect of adding cobalt nanograins in WO_3 sensors, where a similar behavior is observed for 3Co and 4Co films. In their study, the cobalt is segregated in the grain boundaries of WO_3 forming cobalt oxides species and provoking a p-type gas sensor response, contrary to the n-type behavior expected for WO_3 semiconductor.

Cobalt oxide (CoO) is a p-type semiconductor, where cobalt is occupying tetrahedral and octahedral sites. When allying our results from XANES and gas sensing, we can suggest the cobalt segregation is the responsible for the p-type transformation of samples 3Co and 4Co. Apparently, the cobalt inclusion into the ZnO Wurtzite phase is attainable until atomic concentrations of 1.8% (0.6% nominal concentration), from which increase of dopant material may result in phase segregation. To understand the possible inclusion and segregation of cobalt, we used the Raman spectroscopy of doped samples and compared them to ZnO undoped sample as well as pure cobalt oxide (CO_3O_4) (Figure 37)

The bands observed at 366 , 433 , 571 and 665 cm^{-1} correspond to the reported values for A1(TO), E2 (high), 1LO and E1(TO) phonons of zinc oxide structure [35-36], [64–66]. Contrary to the expected for dopant incorporation, the cobalt addition does not cause significant

shifts on these peaks (likely due to the similarity of ionic radius of Zn^{2+} and Co^{2+} ions). Nevertheless, the apparent increase in FWHM of E1 (TO) and 1LO peaks may indicate the microstructural disorder of ZnO lattice (or damage of the crystal lattice) caused by the cobalt incorporation into the zinc sites.

      The cobalt addition also introduces other phonon structures that appears clearly after 1.8% cobalt concentration (2Co strips). The additional structures appear at 482, 520, 554 and 610 cm^{-1} increasing their intensity and evolving into sharper peaks with the cobalt concentration.
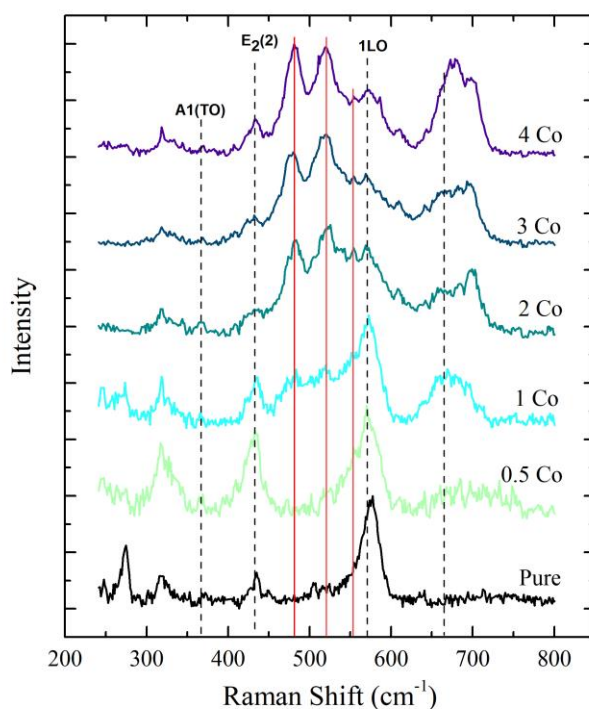
Figure 37 Raman spectra of Co-doped ZnO films compared with the pure ZnO. Source: by the author.

      Baghdad et al. affirms that the appearance of peaks at 470 cm^{-1} 540 cm^{-1} is an indicator of cobalt substituting zinc in lattice sites and these modes are directly related to the loss of vibration symmetry of local vibrations involving the Co atoms [65]. On the other hand, Zhou et al. performed the cobalt-doping of zinc oxide thin films and found that peaks between 470-550 cm^{-1} and 610-630 cm^{-1} (that appears in our samples only at cobalt concentrations higher that 1% (1 Co strip), are associated to the cobalt oxide segregation at the spinel structure Co_3O_4 [66]. Additionally, they report a wide structure observed at region 650-730 cm^{-1} also associated to the presence of spinel structure and other Co related precipitates.

      Besides all of these possible explanations for the Raman spectra of our samples, other

studies of $ZnCo_2O_4$ spinel structure, which is also a p-type semiconductor, demonstrate Raman peaks that are in good agreement with those peaks at region the region between 556 cm^{-1} to 632 cm^{-1} [67,68].

Although is not possible to stablish a decisive conclusion with Raman results about the type of cobalt segregation, it is possible to affirm there is a second phase segregation that was not observed in XRD patters. The cobalt related precipitates (Co_3O_4 or $ZnCo_2O_4$), that have a p-type semiconductor behavior, would be the responsible for the change in type of semiconductor experienced by our sensors when increasing the cobalt concentrations.

4.3.4 Response curve of 2Co sensor as function of ozone concentration

Since the zinc oxide doped sample with two cobalt strips corresponding to 1.8% of atomic cobalt presented, its performance in presence of crescent ozone concentrations is studied (Figure 38). As expected, the gas sensor response is proportional to the ozone presence, demonstrating a linear dependence with the gas concentration. In this case, the variation of response with the gas concentration is lower than the observed for pure material and differently from the others sensor responses, there is a change in the baseline of electrical resistance after each ozone exposure. After ozone detection, the sensor does not recover its initial value but present a decrease in its resistivity, which probably is an evidence of sensor irreversible reaction with ozone.
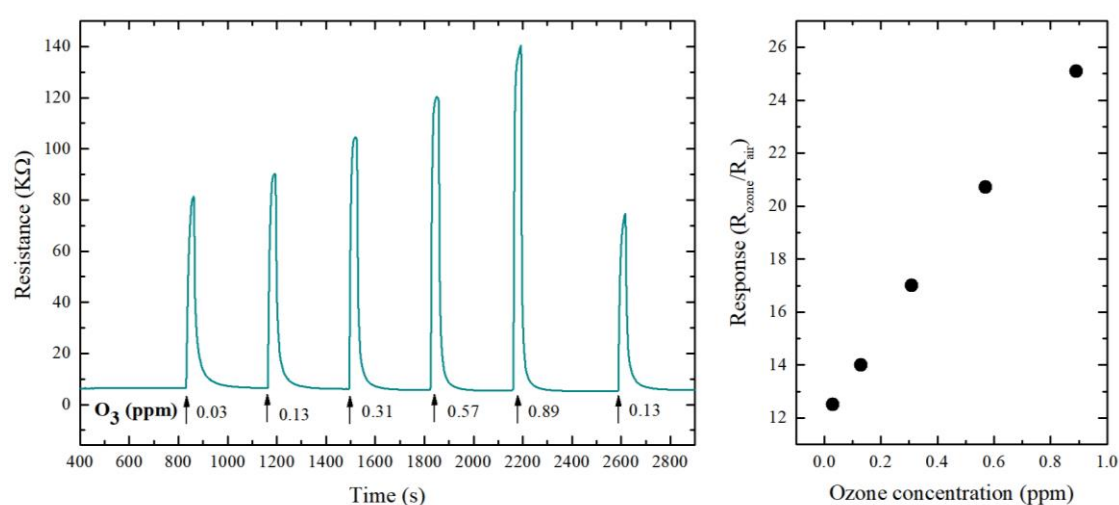
Figure 38 Resistance of 2Co sensor when submitted to consecutive increasing ozone concentrations (left) and gas sensing response as function of the ozone concentration (right). Source: by the author.

5 CONCLUSIONS

This work presents the gas sensing performance of sputtered zinc oxide thin films deposited with different growth conditions, target materials and dopants. The pure zinc oxide morphology and the dopant concentration are studied in order to understand the zinc oxide sensing mechanism and elucidate how the different films react to the presence of ozone.

The target type used for ZnO films production influences the final morphology of ZnO structures and the sensor response to ozone. The ceramic target produces compact and organized structures, while metallic targets create films with low density and great porosity. The sputtering of metal targets increases the deposition rate producing highly porous films which structure reflects on the response: while the response of the sensor produced with the ceramic target is limited up to 1.7 at 0.13 ppm of O_3, the porous film, produced by metallic sputtering followed by thermal oxidation, can reach responses up to 14.

Moreover, the deposition power also controls the dynamics of the sputtering process, showing to have a great effect in the size and porosity of zinc oxide films deposited with metallic target. The deposited films showed to have structures sizes and porosities proportional to the deposition power; aspect that settles the energy of the argon atoms (controlled by the deposition power) as a tuning factor. Lower deposition powers tend to create smaller and compact structures with low response and fast response time. On the other hand, the highest deposition powers create bigger structures with low response and slower response time. In our system, it was possible to achieve the best condition of porosity and structure size that maximize the sensor response at 60W, with the response of circa 14 at 0.13 ppm of O_3.

The doping with cobalt was achieved by insert strips of this metal on the top of zinc target. EDX and XPS data show similar levels of cobalt, although they are a little bit higher than calculated. XANES data suggest that cobalt is occupying a tetrahedric or tetrahedric/octahedric symmetry site. Concentrations lower than 1.8% at. of cobalt (2Co strips) produced a n-type semiconductor, where the 2Co sensor produced a response of circa 19 at 0.13 ppm of O_3, an increment of 62% of the pure zinc oxide sensor. Higher concentrations of cobalt produce a p-type semiconductor and drastically decrease the response magnitude. These results allied with Raman spectroscopy suggest that a phase segregation is taking place at the sensors surface.

6 REFERENCES

1. Batzill, M. Surface science studies of gas sensing materials: SnO₂. *Sensors* **6,** 1345–1366 (2006).

2. Wang, C., Yin, L., Zhang, L., Xiang, D. & Gao, R. Metal Oxide Gas Sensors: Sensitivity and Influencing Factors. *MDPI Sensors* 2088–2106 (2010). doi:10.3390/s100302088

3. Barsan, N., Koziej, D. & Weimar, U. Metal oxide-based gas sensor research : How to ? *Sensors Actuators B Chem.* **121,** 18–35 (2007).

4. Comini, E. Metal oxide nanowire chemical sensors: Innovation and quality of life. *Mater. Today* **19,** 559–567 (2016).

5. Righettoni, M. *et al.* Breath acetone monitoring by portable Si:WO 3 gas sensors. *Anal. Chim. Acta* **738,** 69–75 (2012).

6. Righettoni, M., Tricoli, A. & Pratsinis, S. E. Si : WO 3 Sensors for Highly Selective Detection of Acetone for Easy Diagnosis of Diabetes by Breath Analysis. *Anal. Chem.* **82,** 3581–3587 (2010).

7. Jones, T. A. Semiconductor gas sensors. *Solid State Gas Sensors* 51–69 (1987). doi:10.1016/0250-6874(81)80054-6

8. Lippmann, M. HEALTH EFFECTS OF OZONE A Critical Review. *JAPCA* **39,** 672–695 (1989).

9. Devlin, R. B. *et al.* Exposure of Humans to Ambient Levels of Ozone for 6.6 Hours Causes Cellular and Biochemical Changes in the Lung. *Am. J. Respir. Cell Mol. Biol.* **4,** 72–81 (1991).

10. Block, M. L. & Calderón-Garcidueñas, L. Air pollution: mechanisms of neuroinflammation and CNS disease. *Trends Neurosci.* **32,** 506–516 (2009).

11. Organization, W. health. Ambient (outdoor) air quality and health. Available at: http://www.who.int/mediacentre/factsheets/fs313/en/. (Accessed: 1st February 2017)

12. Barsan, N. & Weimar, U. Conduction model of metal oxide gas sensors. *J. Electroceramics* **7,** 143–167 (2001).

74

13. Özgür, Ü. *et al.* A comprehensive review of ZnO materials and devices APPLIED PHYSICS REVIEWS A comprehensive review of ZnO materials and devices. *J. Appl. Phys.* **41301,** (2005).

14. Liu, L. *et al.* Improve selective acetone sensing properties of Co-doped ZnO nanofibers by electrospining. *Sensors Actuators B. Chem.* 782–788 (2011). doi:https://doi.org/10.1016/j.snb.2011.01.047

15. Darvishnejad, M. H. *et al.* Highly sensitive and selective ethanol and acetone gas sensors by adding some dopants (Mn, Fe, Co, Ni) on hexagonal ZnO plates. *J. Phys. Chem. C* **26,** 7838–7845 (2014).

16. Belkacem, W., Labidi, A., Gu, J., Mliki, N. & Aguir, K. Cobalt nanograins effect on the ozone detection by WO 3 sensors. **132,** 196–201 (2008).

17. Kim, H.-J. & Lee, J.-H. Highly sensitive and selective gas sensors using p-type oxide semiconductors: Overview. *Sensors Actuators B Chem.* **192,** 607–627 (2014).

18. Moon, C. S., Kim, H. R., Auchterlonie, G., Drennan, J. & Lee, J. H. Highly sensitive and fast responding CO sensor using SnO2 nanosheets. *Sensors Actuators, B Chem.* **131,** 556–564 (2008).

19. Alenezi, M. R., Henley, S. J., Emerson, N. G. & Silva, S. R. P. From 1D and 2D ZnO nanostructures to 3D hierarchical structures with enhanced gas sensing properties. *Nanoscale* **6,** 235–247 (2014).

20. Da Silva, L. F. *et al.* Acetone gas sensor based on alpha-Ag2WO4 nanorods obtained via a microwave-assisted hydrothermal route. *J. Alloys Compd.* **683,** 186–190 (2016).

21. Shao, C., Chang, Y. & Long, Y. High performance of nanostructured ZnO film gas sensor at room temperature. *Sensors Actuators, B Chem.* **204,** 666–672 (2014).

22. Korotcenkov, G., Cho, B. K. & Brinzari, V. The Role of Grain Size in Response of SnO 2 - and In 2 O 3 -based Conductometric Gas Sensors. *Adv. Mater. Res.* **486,** 153–159 (2012).

23. Ellmer, K. Magnetron sputtering of transparent conductive zinc oxide: relation between the sputtering parameters and the electronic properties. *J. Phys. D. Appl. Phys.* **33,** R17–R32 (2000).

24. Zhu, L. & Zeng, W. Physical Room-temperature gas sensing of ZnO-based gas sensor :

A review. *Sensors Actuators A. Phys.* **267,** 242–261 (2017).

25. Tao, J. & Batzill, M. *Metal Oxide Nanomaterials for Chemical Sensors.* (2013). doi:10.1007/978-1-4614-5395-6

26. Maeng, S. *et al.* SnO2 nanoslab as NO2 sensor: Identification of the NO2 sensing mechanism on a SnO2 surface. *ACS Appl. Mater. Interfaces* **6,** 357–363 (2014).

27. Fine, G. F., Cavanagh, L. M., Afonja, A. & Binions, R. Metal oxide semi-conductor gas sensors in environmental monitoring. *Sensors* **10,** 5469–5502 (2010).

28. Naisbitt, S. C., Pratt, K. F. E., Williams, D. E. & Parkin, I. P. A microstructural model of semiconducting gas sensor response: The effects of sintering temperature on the response of chromium titanate (CTO) to carbon monoxide. *Sensors Actuators B Chem.* **114,** 969–977 (2006).

29. Seiyama, T., Fujiishi, K., Nagatani, M. & Kato, A. A New Detector for Gaseous Components Using Zinc Oxide Thin Films. *J. Soc. Chem. Ind. Japan* **66,** 652–655 (1962).

30. Jagadish, C. & Pearton Stephen. *Zinc Oxide Bulk, Thin Films and Nanostructures.* (Elseiver Science, 7931).

31. Wöll, C. The chemistry and physics of zinc oxide surfaces. *Prog. Surf. Sci.* **82,** 55–120 (2007).

32. Fan, J. C., Sreekanth, K. M., Xie, Z., Chang, S. L. & Rao, K. V. Progress in Materials Science p-Type ZnO materials : Theory , growth , properties and devices. *Prog. Mater. Sci.* **58,** 874–985 (2013).

33. Norton, M. I. *et al.* Structure and magnetism of cobalt-doped ZnO thin films. *New J. Phys.* **10,** (2008).

34. Alkahlout, A., Dahoudi, N. Al, Grobelsek, I., Jilavi, M. & Oliveira, P. W. De. Synthesis and Characterization of Aluminum Doped Zinc Oxide Nanostructures via Hydrothermal Route. *J. Mater.* **2014,** (2014).

35. Lung, C., Toma, M., Pop, M., Marconi, D. & Pop, A. Characterization of the structural and optical properties of ZnO thin fi lms doped with Ga , Al and (Al þ Ga). *J. Alloys Compd.* **725,** 1238–1243 (2017).

36. Phan, T. L., Vincent, R., Cherns, D., Nghia, N. X. & Ursaki, V. V. Raman scattering in

Me-doped ZnO nanorods (Me = Mn , Co , Cu and Ni) prepared by thermal diffusion. *IOPscience* **475702,** (2008).

37. Ji, S. & Ye, C. Synthesis, Growth Mechanism, and Applications of Zinc Oxide Nanomaterials. *J. Mater. Sci. Technol.* **24,** 457–472 (2008).

38. Seong-Hwan, K., Gyu-In, S. & Se-Young, C. Fabrication of Nb-doped ZnO nanowall structure by RF magnetron sputter for enhanced gas-sensing properties. *J. Alloys Compd.* **698,** 77–86 (2017).

39. Maswanganye, M. W., Rammutla, K. E., Mosuang, T. E. & Mwakikunga, B. W. The effect of Co and In combinational or individual doping on the structural, optical and selective sensing properties of ZnO nanoparticles. *Sensors Actuators B Chem.* (2017). doi:10.1016/j.snb.2017.02.039

40. Xu, J., Pan, Q. & Tian, Z. Grain Size Control and Gas Sensing Properties of ZnO Gas Sensor. *Sensors Actuators B Chem.* **4005,** (2000).

41. Hjiri, M. *et al.* Sensors and Actuators B : Chemical Al-doped ZnO for highly sensitive CO gas sensors. *Sensors Actuators B. Chem.* **196,** 413–420 (2014).

42. Dai, L. *et al.* Chemical High-temperature NO 2 sensor based on aluminum / indium co-doped lanthanum silicate oxyapatite electrolyte and cobalt-free perovskite oxide sensing electrode. *Sensors Actuators B. Chem.* **250,** 629–640 (2017).

43. Catto, A. C. *et al.* Local Structure and Surface Properties of CoxZn1-xO Thin Films for Ozone Gas Sensing. *ACS Appl. Mater. Interfaces* **8,** 26066–26072 (2016).

44. Jackson, G. N. R.F. Sputtering. *Thin Solid Films* **5,** 209–246 (1970).

45. CasaXPS software Ltd.

46. AlainMichalowicz. Cherokee. (2013).

47. Ohring, M. *Materials Science of Thin Films, Second Edition*. *Materials Science* (2001). doi:10.1016/B978-0-12-524975-1.50018-5

48. Ruffino, F. & Torrisi, V. Ag films deposited on Si and Ti: How the film-substrate interaction influences the nanoscale film morphology. *Superlattices Microstruct.* **111,** 81–89 (2017).

49. Mihailova, I. *et al.* Synthesis of ZnO nanoneedles by thermal oxidation of Zn thin films. *J. Non. Cryst. Solids* **377,** 212–216 (2013).

50. Khanlary, M. R., Vahedi, V. & Reyhani, A. Synthesis and characterization of ZnO nanowires by thermal oxidation of zn thin films at various temperatures. *Molecules* **17,** 5021–5029 (2012).

51. Zhao, J. *et al.* High-quality ZnO thin films prepared by low temperature oxidation of metallic Zn. *Appl. Surf. Sci.* **229,** 311–315 (2004).

52. Schuler, L. P., Alkaisi, M. M., Miller, P., Reeves, R. J. & Markwitz, A. Comparison of DC and RF sputtered zinc oxide films with post-annealing and dry etching and effect on crystal composition. *Japanese J. Appl. Physics, Part 1 Regul. Pap. Short Notes Rev. Pap.* **44,** 7555–7560 (2005).

53. Nandi, R. & Major, S. S. The mechanism of growth of ZnO nanorods by reactive sputtering. *Appl. Surf. Sci.* **399,** 305–312 (2017).

54. Laurenti, M. *et al.* RSC Advances A porous nanobranched structure : an e ff ective way to improve piezoelectricity in sputtered ZnO thin. 76996–77004 (2016). doi:10.1039/C6RA17319E

55. Raimondi, D. L. & Kay, E. High Resistivity Transparent ZnO Thin Films. **96,** (2010).

56. Lu, L., Wong, M. & Member, S. The Resistivity of Zinc Oxide Under Different Annealing Configurations and Its Impact on the Leakage Characteristics of Zinc Oxide Thin-Film Transistors. **61,** 1077–1084 (2014).

57. Ismail, A. & Abdullah, M. J. The structural and optical properties of ZnO thin films prepared at different RF sputtering power. *J. King Saud Univ. - Sci.* **25,** 209–215 (2013).

58. Somorjai, G. A. *fundamentos de química de superficies*. (Alhambra, 1975).

59. Zhang, J. *et al.* Hierarchically Porous ZnO Architectures for Gas Sensor Application & DESIGN 2009. 5–10 (2009).

60. Zhu, J. *et al.* Hierarchical porous/hollow tin oxide nanostructures mediated by polypeptide: Surface modification, characterization, formation mechanism and gas-sensing properties. *Nanotechnology* **17,** 5960–5969 (2006).

61. Li, C. *et al.* Phase and composition controllable synthesis of cobalt manganese spinel nanoparticles towards efficient oxygen electrocatalysis. *Nat. Commun.* **6,** 1–8 (2015).

62. Gandhi, V., Ganesan, R., Hameed, H., Syedahamed, A. & Thaiyan, M. E ff ect of

Cobalt Doping on Structural, Optical, and Magnetic Properties of ZnO Nanoparticles Synthesized by Coprecipitation Method. *J. Phys. Chem.* (2014).

63. Li, Y. F. *et al.* Realization of p -type conduction in undoped Mg x Zn 1 − x O thin films by controlling Mg content Realization of p -type conduction in undoped Mg x Zn 1 − x O thin films. *Appl. Phys. Lett.* **232115,** (2013).

64. Ashkenov, N. *et al.* Infrared dielectric functions and phonon modes of high-quality ZnO films. *J. Appl. Phys.* **126,** (2003).

65. Baghdad, R., Lemér, N., Lamura, G., Zeinert, A. & Hadj-zoubir, N. Superlattices and Microstructures Structural and magnetic properties of Co-doped ZnO thin fi lms grown by ultrasonic spray pyrolysis methoLamura, Gd. *Superlattices Microstruct.* **104,** (2017).

66. Zhou, H. *et al.* Raman studies of ZnO : Co thin films. *Phys. Status Solidi a* **117,** 112–117 (2007).

67. Morán-Lázaro, J. *et al.* Synthesis, Characterization, and Sensor Applications of Spinel ZnCo2O4 Nanoparticles. *Sensors* **16,** 2162 (2016).

68. Zhou, X. *et al.* Highly sensitive acetone gas sensor based on porous ZnFe2O4 nanospheres. *Sensors Actuators, B Chem.* **206,** 577–583 (2015).